ligation to produce MI. The surgical procedures are described in detail elsewhere (28). Briefly, after pentobarbital sodium anesthesia (25–40 mg/kg ip) and intubation with a polyethylene tube (size 60), animals were ventilated by using a volume-cycled rodent respirator with 2 to 3 ml/cycle at a respiratory rate of 120 breaths/min. After thoracotomy, the LCA was ligated with a suture, 3 to 4 mm from the tip of the left auricle. The chest wall and skin were closed with a suture. The same surgical procedures were performed in sham mice, except that the coronary artery was not ligated.

*LV morphology and morphometry.* Four weeks after LCA ligation, the left ventricle (LV), including the septum, and the right ventricle were dissected to confirm MI in some groups of mice. After the major long-axis intracavitary diameter was measured, each LV was serially sectioned into three rings perpendicular to the major axis of the heart, after which the short-axis diameter was measured. At the midregion, the minimal and maximal chamber diameters were used with the long-axis diameter to compute the LV chamber volume. Infarct size in these hearts was determined by the method described previously (40). Briefly, serial 5-μm sections were prepared, mounted, and stained with Masson trichrome. Infarct length was measured along the endo- and epicardial surfaces from each of the three LV sections, and values from all three sections were summed. Total LV circumference was calculated as the sum of the endo- and epicardial segment lengths from all three sections. Infarct size (in %) was calculated as the total infarct circumference divided by the total circumference times 100.

*Measurement of blood pressure and heart rate during intracisternal administration of L-NMMA.* In a separate group of animals, we examined the effects of intracisternal injection of $N^G$-monomethyl-L-arginine (L-NMMA), a NOS inhibitor, on blood pressure in the MI and sham-operated mice ($n$ = 6 mice each) to confirm that the NOS activity was altered in MI mice. Four weeks after LCA ligation, the mice were anesthetized with pentobarbital sodium (50 mg/kg ip) and mechanically ventilated with room air supplemented with oxygen. A catheter was introduced into the left femoral vein for the administration of anesthetics. Another catheter was introduced into the aorta through the femoral artery to monitor and record systemic arterial pressure. The mice were placed in a stereotaxic frame, the dorsal surface of the medulla was then exposed, and the tip of a polyethylene tube (PE-10) was placed into the cisterna magna. Bolus injections of L-NMMA (100 nmol, 10 μl) were made through this tube. The drugs were dissolved in artificial cerebrospinal fluid containing (in mM) 123 NaCl, 0.86 $CaCl_2$, 3.0 KCl, 0.89 $MgCl_2$, 25 $NaHCO_3$, 0.5 $NaH_2PO_4$, and 0.25 $Na_2HPO_4$; pH 7.4.

*Construction and purification of recombinant adenovirus.* We used adenoviral vectors encoding either the bacterial β-galactosidase (Adβgal) gene or bovine endothelial NOS (eNOS) gene (6, 30). A replication-deficient adenovirus encoding the bovine eNOS gene expressed from a long-terminal repeat of the *Rous sarcoma* virus as a promoter was generated by using standard methods from the University of Iowa Gene Transfer Vector Core (Iowa City, IA) (6, 30). These vectors were suspended in PBS with 3% sucrose and stored at −80°C until use.

*In vivo gene transfer into NTS.* Four weeks after LCA ligation, mice were anesthetized with pentobarbital sodium (25–40 mg/kg ip), placed on a stereotaxic frame, and the dorsal surface of the medulla was exposed. A glass micropipette (5 μm, outer diameter) was filled with PBS containing Adβgal or AdeNOS. Bilateral injections were made into the NTS. One microinjection site in each NTS was defined according to a mouse atlas (35). An adenoviral suspension containing $1 \times 10^8$ plaque forming units per milliliter was injected into each injection site over 10 min (200 nl/each NTS; infusion rate, ~40 nl/min). After the injection, all mice recovered from the anesthesia and were unrestrained and free to move in their cages.

*Histochemical analysis of β-galactosidase gene expression.* On *day 7* after the gene transfer, the mice were deeply anesthetized with pentobarbital sodium (100 mg/kg ip) and perfused transcardially with PBS, followed by 4% paraformaldehyde in PBS. The brains were removed, and the coronal sections of the medulla were cut serially (50 μm) using a vibratome. The sections of the medulla were evaluated for β-galactosidase expression by histostaining with X-Gal in PBS at 37°C for 4 h.

*Quantification of β-galactosidase activity.* We quantified β-galactosidase activity in the mice ($n$ = 4 mice at each time point) transfected with Adβgal with a colorimetric assay using *o*-nitrophenyl-β-D-galactopyranosidase (Boehringer Mannhein Biochemica; Mannheim, Germany) as described previously (2, 9, 17), before and on *days 1, 3, 5, 7, 10, 14, 21,* and *28* after the transfection of Adβgal.

*Immunohistochemistry for eNOS and nNOS.* In another group of animals, sheep anti-nNOS antibody (kindly provided by P. Emson, Department of Neurobiology, The Babraham Institute, Cambridge, UK) was used for an immunohistochemical analysis of endogenous nNOS (19). Four weeks after LCA ligation, serial sections of the medulla were obtained. The sections were incubated in sheep anti-nNOS antibody (1:10,000) and then rinsed in PBS. After overnight incubation in biotinylated donkey anti-sheep IgG (1:1,000, Jackson; Baltimore, MD), the sections were rinsed in PBS and incubated in a mixture of streptavidin-conjugated fluorescein isothiocyanate (1:200; Vector; Burlingame, CA). After being rinsed in PBS, the sections were mounted in Vectashield (Vector). In a separate group of mice transfected with AdeNOS, we performed immunohistochemistry for eNOS as described previously (22, 39). On *day 7* after the gene transfer, the sections were incubated in rabbit anti-eNOS IgG (1:200; Transduction; Lexington, KY) at room temperature overnight and then rinsed three times in PBS. After incubation with biotinylated horse anti-rabbit IgG (1:1,000, Vector), the sections were rinsed in PBS and incubated in a mixture of streptavidin-conjugated rhodamine (1:100, Vector). After being rinsed in PBS, the sections were mounted in Vectashield (Vector). The stained sections were photographed by using a confocal laser scanning microscope (MRC 1000, Bio-Rad; mounted on a Nikon light microscope Optiphot, Hemel Hempstead, UK) using laser beams of 488 nm for nNOS-stained sections and 580 nm for eNOS-stained sections for excitation with appropriate filter sets. Confocal images were then transferred to a personal computer and analyzed by using the National Institutes of Health Image program.

*Western blot analysis for eNOS and nNOS.* We performed Western blot analysis to determine the level of endogenous nNOS protein expression in MI mice. We also performed Western blot analysis to determine the time course of eNOS protein expression in AdeNOS-transfected mice. A coronal block of the brain ($n$ = 4 mice for each line) containing the NTS was dissected, and the NTS tissues were obtained by using the punch microdissection technique (32, 33, 41) in MI mice and AdeNOS-transfected mice at 4 wk after LCA ligation and on *days 0, 3, 5, 7, 10, 14,* and *28* after AdeNOS transfer, respectively. The NTS tissues were homogenized and sonicated in a lysis buffer containing 40 mmol/l HEPES, 1% Triton X-100, 10% glycerol, and 1 mmol/l phenylmethylsulfonyl fluoride. The tissue lysate was centrifuged at 6,000 rpm for 5 min at 4°C using a microcentrifuge. The supernatant was collected, and the protein concentration was determined by using a bicinchoninic acid protein assay kit (Pierce Chemical; Rockford, IL). An aliquot of 5 μg of protein from each sample was separated on a sodium dodecyl sulfate gel and transferred electrophoretically onto polyvinylidene difluoride membranes (Immobilon-P membrane; Millipore, Bedford, MA). After we confirmed that equal amounts of protein were applied into each well using Ponceau S (Sigma Chemical, St. Louis, MO) staining, the membranes were incubated with either sheep anti-nNOS antibody (1:10,000) in MI mouse samples or rabbit anti-eNOS (1:200) in AdeNOS-transfected mouse samples. Membranes were then washed and incubated with a horseradish peroxidase conjugated horse anti-sheep IgG antibody (1:10,000) or horse anti-rabbit IgG (1:100,000), respectively. Immunoreactivity was detected by enhanced chemiluminescence autoradiography (ECL Western blotting detection kit; Amersham; Arlington Heights, IL).

*Echocardiographic imaging.* Four weeks after LCA ligation, i.e., just before the adenoviral gene transfer, serial two-dimensional and M-mode echocardiography was performed in all groups of animals under light pentobarbital sodium anesthesia with spontaneous respiration (15). An echocardiography system (SSD5000; Aloka, Tokyo) was used with a dynamically focused 10-MHz linear array transducer using a depth setting of 200 mm, as described previously (15, 28). Two-dimensional images and M-mode tracings were recorded from the short-axis view at the level of the papillary muscle. Care was taken to avoid applying too much pressure to the chest wall. The M-mode tracings were printed on glossy paper using a digital color printer (SSZ337). LV end-diastolic diameter (LVEDD), LV end-systolic diameter (LVESD), and wall thickness were measured, and the mean of three-to-five cardiac cycles was used for analysis. Percent fractional shortening (%FS) was calculated as follows: %FS = (LVEDD) − (LVESD)/(LVEDD) × 100. The same echocardiographic experiments were performed 6 and 8 wk after LCA ligation, i.e., 2 and 4 wk after AdeNOS gene transfer, respectively.

*Measurement of urinary norepinephrine excretion.* The urinary norepinephrine concentration was measured 4 wk after LCA ligation, i.e., just before gene transfer, and 7 days after the gene transfer by high-performance liquid chromatography, and urinary norepinephrine excretion over 24 h (μg/day) was then calculated as described previously (17, 22, 39).

*Statistical analysis.* All values were expressed as means ± SE. One-way ANOVA was used to compare the β-galactosidase activity. An unpaired *t*-test was used to compare values between the MI mice and sham-operated mice. Two-way ANOVA with repeated measures was used to compare the time course values of LVEDD and %FS between Adβgal and AdeNOS-transfected MI mice groups. A paired *t*-test was used to compare the values before and after each operation, or before and after the gene transfer, in sham-operated and MI mice. Differences were considered to be significant when $P < 0.05$.

## RESULTS

*HF characteristics of MI mice.* Echocardiographic assessment of cardiac function was performed, and infarct size was estimated using Masson trichrome staining before and 4 wk after LCA ligation. Echocardiographic evaluation revealed that LVEDD was greater (5.2 ± 0.4 vs. 3.6 ± 0.2 mm; $P < 0.01$) and fractional shortening was smaller (19.1 ± 0.2% vs. 42.7 ± 0.1%; $P < 0.01$) in MI mice than in sham-operated mice ($n$ = 11, each group) (Fig. 1, *A* and *B*). Examples of coronal sections of the LV are shown in Fig. 1, *C* and *D*. Infarct size of MI mice was 42.5 ± 2.3% (see Fig. 1, *C* and *D*). Furthermore, 24-h urinary norepinephrine excretion was significantly higher in MI mice compared with that in sham-operated mice (MI mice, 0.33 ± 0.06 μg; sham mice, 0.18 ± 0.03 μg; $n$ = 13 mice for each group, $P < 0.05$). There was no difference in 24-h urinary volume between MI mice and sham-operated mice (data not shown).

*Brain stem nNOS is reduced in HF.* In this model, we evaluated nNOS protein expression in the brain stem by Western blot analysis and immunohistochemistry 4 wk after LCA ligation. Western blot analysis for nNOS in the NTS revealed reduced nNOS protein levels in MI mice compared with sham-operated mice (Fig. 2*A*). Immunohistochemical staining for nNOS protein was reduced in MI mice compared with that in sham-operated mice (Fig. 2, *B* and *C*).

*Effect of intracisternal injection of L-NMMA on blood pressure.* To determine whether endogenous NOS activity was altered in MI mice, we examined the effects of intracisternal injection of L-NMMA on blood pressure in sham-operated and

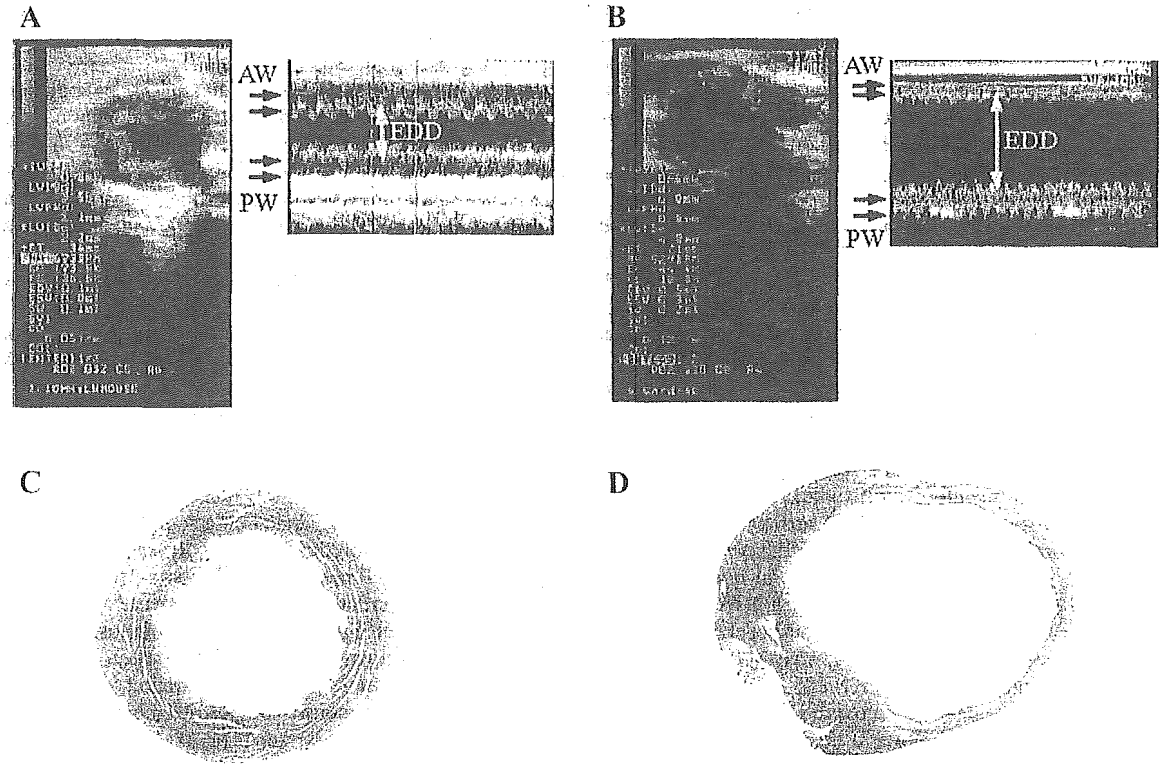


Fig. 1. B-mode and M-mode echocardiograms of left ventricular (LV) in parasternal short-axis view obtained from sham-operated (*A*) and myocardial infarction (MI) (*B*) mice. EDD, end-diastolic diameter; AW, anterior wall; PW posterior wall. MI mice exhibited LV dilatation and decreased fractional shortening. Low-power photograph of Masson-trichrome-stained LV cross-section was obtained from sham-operated (*C*) and MI (*D*) mice.

MI mice. Intracisternal injection of L-NMMA elicited a smaller increase in blood pressure in MI mice than in sham-operated mice (6.9 ± 3.4 vs. 20.6 ± 4.9 mmHg; $P < 0.05$) (Fig. 3*B*).

*Effect of eNOS overexpression in NTS.* Figure 4*A* shows the X-Gal staining for β-galactosidase in a section of the mouse brain medulla on *day 7* after the gene transfer. Positive staining for β-galactosidase was observed in the NTS where Adβgal had been microinjected. In the AdeNOS-transfected mice, eNOS protein expression was observed immunohistochemically in the NTS where AdeNOS had been microinjected (Fig. 4*B*). Figure 4*C* shows the time course of β-galactosidase activity before and after Adβgal transfection. The β-galactosidase activity in the medulla peaked on *day 7* and then declined over time. Figure 4*D* shows the time course of eNOS protein expression as determined by Western blot analysis. eNOS protein expression peaked at *day 7* and then declined over time until *day 28*. Urinary norepinephrine excretion in MI mice transfected with Adβgal or AdeNOS was also measured. Urinary norepinephrine excretion did not differ before adenoviral gene transfer (Fig. 5). Urinary norepinephrine excretion after transfection with AdeNOS, however, was significantly lower than before transfection with AdeNOS. In addition, after the gene transfer, urinary norepinephrine excretion in AdeNOS-transfected MI mice was significantly lower than in Adβgal-transfected MI mice. There was no change in 24-h urinary volume after AdeNOS transfection (data not shown). Adenoviral-mediated eNOS gene delivery did not improve the LV systolic function determined by EDD and %FS (Table 1).

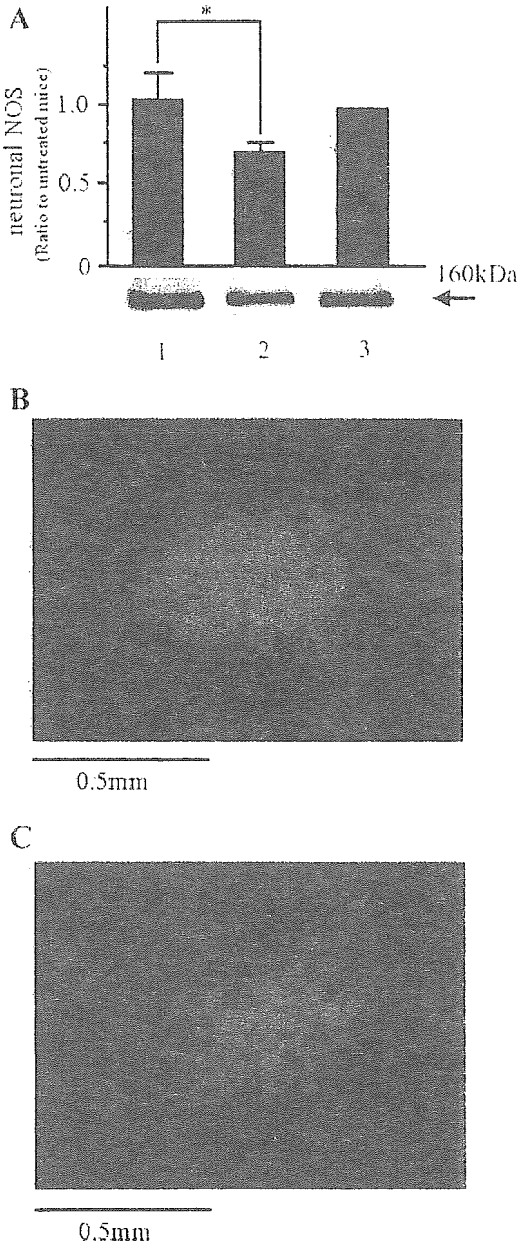


Fig. 2. Western blot analysis in nucleus tractus solitarius (NTS) demonstrating reduction in endogenous neuronal nitric oxide synthase (nNOS) protein in MI mice ($n = 4$ mice for each) *A*: *lane 1*, sham-operated mouse; *lane 2*, MI mouse; *lane 3*, untreated mouse. Immunohistochemical staining visualized with rhodamine-conjugated fluoroprobe for endogenous nNOS protein within NTS tissue in sham-operated (*B*) and MI (*C*) mice. *$P < 0.05$ compared with the value of sham-operated mice.

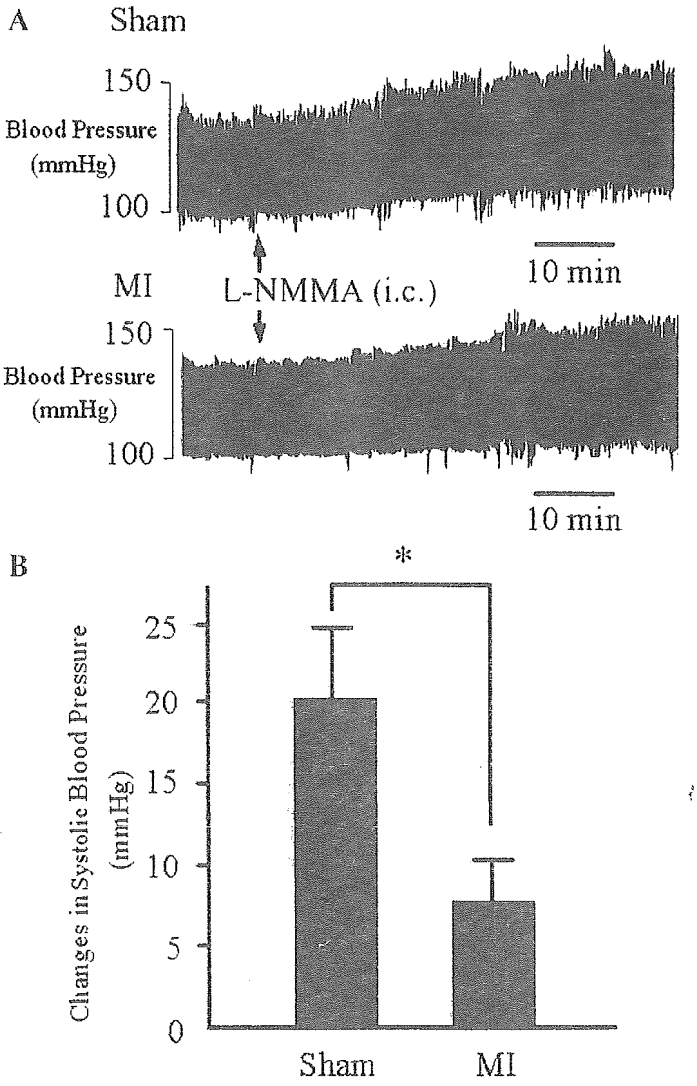


Fig. 3. Typical effects (*A*) and summary (*B*) observed in blood pressure changes after intracisternal (i.c.) injection of $N^G$-monomethyl-L-arginine (L-NMMA) in sham-operated and MI (*B*) mice, suggesting that NOS activity was reduced in MI mice ($n = 6$ mice for each, *$P < 0.05$).

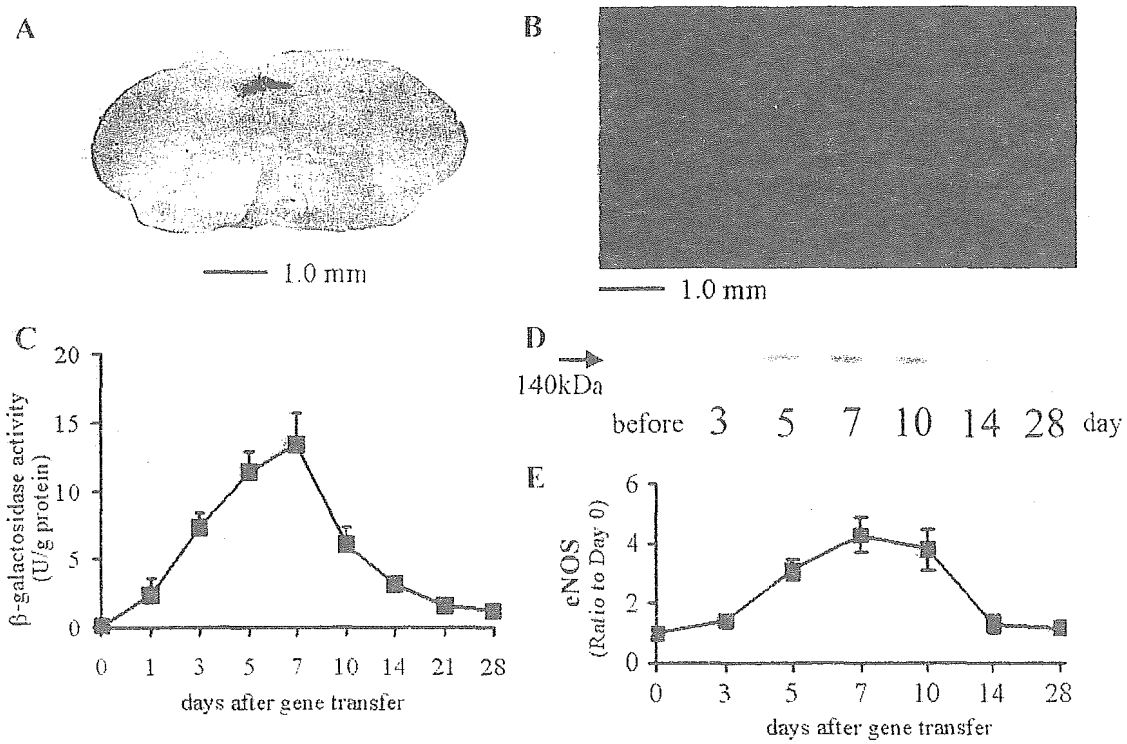


Fig. 4. Site-specific expression of β-galactosidase or endothelial NOS (eNOS) protein within NTS. *A*: dark blue X-Gal staining was observed locally in NTS of Adβgal-transfected mice. *B*: images of section of medulla stained with anti-eNOS antibody (red, visualized with rhodamine-conjugated fluoroprobe). *C*: eNOS-immunopositive sites are also detected locally in bilateral NTS of AdeNOS-injected mice. Time course of β-galactosidase activity in medulla transfected with Adβgal. β-Galactosidase activity was quantified by using colorimetric assay ($n$ = 4 mice at each time point). *D* and *E*: time course of eNOS protein expression in medulla transfected with AdeNOS by Western blot analysis.

## DISCUSSION

The major findings of the present study are as follows. First, the characteristics of MI mice were consistent with those of HF, a particularly increased activation of the sympathetic nervous system as determined by an increase in urinary norepinephrine excretion. Second, nNOS expression levels were significantly reduced in this MI mouse model. Finally, increased NO production induced by eNOS overexpression in the NTS in MI mice reduced urinary norepinephrine excretion to the levels of the sham-operated mice, suggesting that increased NO production in the NTS reduced the enhanced sympathetic drive in MI mice. Taken together, these results indicate that decreased NO in the brain, especially in the NTS, contributes to the enhanced sympathetic drive observed in HF.

*MI mouse model of HF.* HF was produced by coronary artery ligation in mice. This model is often used as a model of LV remodeling, myocardial ischemia, and reperfusion injury (15, 24, 28, 36, 39, 40, 43). Little is known, however, regarding the neurohumoral aspects of this model in mice. In our study, we demonstrated that urinary norepinephrine excretion measured

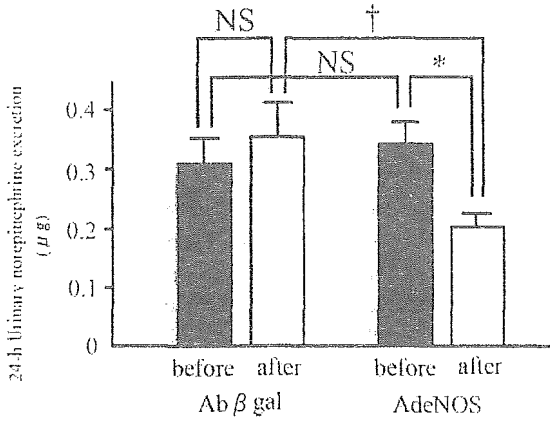


Fig. 5. Twenty-four-hour urinary norepinephrine excretion (in μg) before and after gene transfer in AdeNOS- and Adβgal-transfected MI mice. NS, not significant. *$P < 0.05$; †$P < 0.01$.

Table 1. *Time course of LV end-diastolic diameter and %FS in MI and sham-operated mice transfected with either Adβgal or AdeNOS*

| | Sham Mice | | MI Mice | |
|---|---|---|---|---|
| | AdeNOS | Adβgal | AdeNOS | Adβgal |
| $n$ | 10 | 7 | 9 | 6 |
| | *LV end-diastolic diameter, mm* | | | |
| Before LCA Ligation | 3.7±0.2 | 3.6±0.2 | 5.3±0.3 | 5.2±0.4 |
| 2 Wk | 3.6±0.3 | 3.7±0.3 | 5.3±0.4 | 5.4±0.6 |
| 4 Wk | 3.8±0.3 | 3.8±0.3 | 4.9±0.5 | 5.2±0.9 |
| | *%FS* | | | |
| Before LCA Ligation | 45.5±0.2 | 42.7±0.3 | 19.7±0.9 | 19.1±0.9 |
| 4 Wk | 44.2±0.3 | 44.9±0.3 | 22.7±1.2 | 20.8±1.7 |
| 8 Wk | 39.1±0.4 | 40.5±0.3 | 24.7±1.4 | 19.3±1.5 |

Values are means ± SE; $n$, number of mice. LV, left ventricular; % FS, percent fractional shortening; MI, myocardial infarction; Adβgal and AdeNOS, adenoviral vectors encoding β-galactosidase or endothelial nitric oxide synthase, respectively.

in a conscious state, which is a marker of sympathetic nerve activity, was significantly increased in mice 4 wk after MI. Consistent with the results of previous studies from Takeshita's laboratory (15), LV dilatation and reduced LV systolic function were also observed.

*Sympathoexcitation in HF and role of NO in brain stems.* HF is characterized by an enhanced neurohumoral drive in experimental animals as well as in patients (27, 29, 55). In patients with HF, plasma norepinephrine levels increase with severity and relate to the mortality rate (4, 38). The mechanism(s) underlying the sympathoexcitation observed in HF is not fully understood. Although it has been thought that abnormal arterial baroreflex and cardiopulmonary baroreflex control of sympathetic nerve activity are responsible for the sympathoexcitation in HF, recent studies (27, 29, 55) suggest that involvement of the CNS is important. Many studies (10, 27, 29, 55) predict an important role of angiotensin II, particularly in the forebrain, in HF. Liu and Zucker (25) suggested that a loss of NO and an increase in angiotensin II are necessary for sustained increases in sympathetic nerve activity in HF. In fact, inhibition of angiotensin II type I receptors in the NTS reduces arterial blood pressure, heart rate, and sympathetic nerve activity in rats with chronic inhibition of NOS (8). Previous studies from our laboratories and others (17, 22, 39) have established that NO in the brain inhibits sympathetic nerve activity. There are few studies (34, 54), however, regarding NO in the brain, especially the NTS, in HF. Patel et al. (33) reported decreased nNOS gene mRNA expression levels in the hypothalamus, dorsal pons, and dorsal medulla of rats with MI compared with those in sham-operated rats. In addition, the number of NADPH-diaphorase-positive neurons, a marker of nNOS activity, was significantly decreased in the PVN (54). In animal models of HF, blunted NO inhibition mediated sympathoexcitation in the PVN (53) and reduced central NO-mediated enhanced sympathetic afferent baroreflex gain (26).

In the present study, nNOS expression evaluated by Western blot analysis and immunohistochemical staining in the brain stem, particularly in the NTS, was reduced in HF mice compared with that in sham-operated mice. Also, the pressor response evoked by intracisternal injection of L-NMMA was lower in MI mice compared with that in sham-operated mice, suggesting that NOS activity in the NTS is reduced in our MI mouse model.

*Effect of eNOS overexpression in NTS.* The most important finding of the present study is that the increase in urinary norepinephrine excretion in MI mice was significantly reduced compared with that in the sham-operated mice after eNOS overexpression in the NTS in a conscious state. This finding indicates that an increase in NO production in the NTS normalizes the enhanced sympathetic drive observed in HF. In the present study, we transfected adenoviral vectors encoding either the β-galactosidase gene or the eNOS gene into the NTS of mice in vivo, which was confirmed by Western blot analysis and immunohistochemical staining. Furthermore, consistent with previous studies from Takeshita's laboratory (39) using rats, the time course of β-galactosidase activity or eNOS expression peaked on *day 7* after the gene transfer. Because we (20) and others (44) previously demonstrated that overexpression of eNOS in the brain does not affect the nNOS expression levels, the maximum physiological effect of viral-mediated gene transfer was anticipated to occur on *day 7* after the gene transfer. Therefore, we measured urinary norepinephrine excretion on *day 7* after the gene transfer. As discussed in previous studies (17, 22, 39) using this technique, we used eNOS instead of nNOS, which normally exists in the CNS, because the purpose of this study was to increase the local NO production in the NTS for a relatively long period in mice transfected with AdeNOS. We previously demonstrated that this method is useful for examining the effect of NO overproduction in a specific nucleus of the brain on cardiovascular regulation in conscious animals (17, 22, 39). The increase in NOS expression in the NTS attenuated the increase in urinary norepinephrine excretion, which is a marker of sympathetic nerve activity, in MI mice in a conscious state. These results suggest that the reduced NO production in the NTS contributes to the enhanced sympathetic drive in HF.

Waki et al. (49) reported that chronic inhibition of endogenous eNOS in the caudal NTS enhances baroreflex and suggested that NO might be functionally diverse within the NTS. In the present study, we did not address the role of endogenous NO released from neurons and endothelium (34) on the baroreflex function in HF. There are functionally discrete subregions that exhibit a different response to the same neuropeptide, even within the NTS (45). Thus various results between the caudal subregion of the NTS in the study by Waki et al. (49) and the entire NTS in the present study might reflect the diverse physiological functions of NO based on discrete subgroups of neurons within the NTS.

A recent study (51) indicated that NO in a different brain stem nucleus, the rostral ventrolateral medulla, also improves HF pathophysiology. Therefore, increasing NO in the brain stem might be a new therapeutic target for the treatment of HF from the aspect of neurohumoral activation.

*Study limitations.* It is possible that the reduced blood pressure response to L-NMMA in mice with HF was due to elevated basal sympathetic nerve activity that cannot be further increased. This possibility is unlikely, however, because the sympathetic nerve response to blocking the airway in HF rats was higher than that elicited by L-NMMA (53). Recently, it was suggested that NADPH-dependent superoxide anions are increased in the brain in experimental chronic HF and that increased reactive oxygen species in the brain contribute to increased sympathetic nerve activity (12, 21, 24). Because brain NO might be trapped by increased superoxide anions in chronic HF states, it is possible that the sympathoexcitation in HF is determined by the balance between NO and reactive oxygen species. Further studies are required to elucidate this point.

We found that eNOS gene transfer in the NTS normalized the enhanced sympathetic drive observed in our HF model. We measured urinary norepinephrine excretion as a marker of sympathetic nerve activity. Direct measurement of sympathetic nerve activity is preferable, but it is technically difficult to perform in conscious mice. Because the expression of the gene using adenovirus vectors remains high enough for only several days, this technique does not allow us to observe an improvement in survival (data not shown) or inhibition of LV remodeling (Table 1). Further experiments to examine the long-term effect of an increase in NO within the brain stem in HF are important. Another efficient vector system that expresses the gene for a longer period, such as the adenovirus-associated virus (37) or feline immunodeficiency virus (42),

might be useful for examining the long-term effect of NO in the NTS on HF.

In conclusion, MI mice have characteristics consistent with HF, particularly from the aspect of sympathetic nervous system activation. This activation is mediated, at least in part, by decreases in nNOS expression, resulting in decreased NO production in the NTS. Overexpression of eNOS in the NTS decreases urinary norepinephrine excretion, suggesting that increased NO production in the brain stem, particularly in the NTS, reduces the enhanced sympathetic drive observed in HF.

## ACKNOWLEDGMENTS

The authors thank Drs. D. D. Heistad and B. L. Davidson (The University of Iowa Gene Transfer Vector Core, supported by National Institutes of Health grants and the Carver Foundation) for the preparation of vectors. We thank Dr. P. Emson for kindly providing the sheep antibody to nNOS. We also thank Dr. T. Kosaka for advice in the immunohistochemical analysis for eNOS and the use of his facility for microscopic analysis.

## GRANTS

This work was supported by a Grant-in-Aid for Scientific Research (C11670689) from the Ministry of Education, Science, Sports, and Culture and the Japan Society for the Promotion of Science.

## REFERENCES

1. **Andresen MC and Kunze DL.** Nucleus tractus solitarius–gateway to neural circulatory control. *Annu Rev Physiol* 56: 93–116, 1994.
2. **Bradford MM.** A rapid and sensitive method for the quantitation of microgram quantities of protein utilizing the principle of protein-dye binding. *Anal Biochem* 72: 248–254, 1976.
3. **Bristow MR, O'Connell JB, Gilbert EM, French WJ, Leatherman G, Kantrowitz NE, Orie J, Smucker ML, Marshall G, and Kelly P.** Dose-response of chronic beta-blocker treatment in heart failure from either idiopathic dilated or ischemic cardiomyopathy. Bucindolol Investigators. *Circulation* 89: 1632–1642, 1994.
4. **Cohn JN, Levine TB, Olivari MT, Garberg V, Lura D, Francis GS, Simon AB, and Rector T.** Plasma norepinephrine as a guide to prognosis in patients with chronic congestive heart failure. *N Engl J Med* 311: 819–823, 1984.
5. **Dampney RA.** Functional organization of central pathways regulating the cardiovascular system. *Physiol Rev* 74: 323–364, 1994.
6. **Davidson BL, Allen ED, Kozarsky KF, Wilson JM, and Roessler BJ.** A model system for in vivo gene transfer into the central nervous system using an adenoviral vector. *Nat Genet* 3: 219–223, 1993.
7. **De Vente J, Hopkins DA, Markerink-Van Ittersum M, Emson PC, Schmidt HH, and Steinbusch HW.** Distribution of nitric oxide synthase and nitric oxide-receptive, cyclic GMP-producing structures in the rat brain. *Neuroscience* 87: 207–241, 1998.
8. **Eshima K, Hirooka Y, Shigematsu H, Matsuo I, Koike G, Sakai K, and Takeshita A.** Angiotensin in the nucleus tractus solitarii contributes to neurogenic hypertension caused by chronic nitric oxide synthase inhibition. *Hypertension* 36: 259–263, 2000.
9. **Eustice DC, Feldman PA, Colberg-Poley AM, Buckery RM, and Neubauer RH.** A sensitive method for the detection of beta-galactosidase in transfected mammalian cells. *Biotechniques* 11: 739–740, 1991.
10. **Felder RB, Francis J, Weiss RM, Zhang ZH, Wei SG, and Johnson AK.** Neurohumoral regulation in ischemia-induced heart failure. Role of the forebrain. *Ann NY Acad Sci* 940: 444–453, 2001.
11. **Francis GS, Benedict C, Johnstone DE, Kirlin PC, Nicklas J, Liang CS, Kubo SH, Rudin-Toretsky E, and Yusuf S.** Comparison of neuroendocrine activation in patients with left ventricular dysfunction with and without congestive heart failure. A substudy of the Studies of Left Ventricular Dysfunction (SOLVD). *Circulation* 82: 1724–1729, 1990.
12. **Gao L, Wang W, Li YL, Schultz HD, Liu D, Cornish KG, and Zucker IH.** Superoxide mediates sympathoexcitation in heart failure: roles of angiotensin II and NAD(P)H oxidase. *Circ Res* 95: 937–944, 2004.
13. **Hara H, Waeber C, Huang PL, Fujii M, Fishman MC, and Moskowitz MA.** Brain distribution of nitric oxide synthase in neuronal or endothelial nitric oxide synthase mutant mice using [$^3$H]L-$N^G$-nitro-arginine autoradiography. *Neuroscience* 75: 881–890, 1996.
14. **Harada S, Tokunaga S, Momohara M, Masaki H, Tagawa T, Imaizumi T, and Takeshita A.** Inhibition of nitric oxide formation in the nucleus tractus solitarius increases renal sympathetic nerve activity in rabbits. *Circ Res* 72: 511–516, 1993.
15. **Hayashidani S, Tsutsui H, Shiomi T, Suematsu N, Kinugawa S, Ide T, Wen J, and Takeshita A.** Fluvastatin, a 3-hydroxy-3-methylglutaryl coenzyme a reductase inhibitor, attenuates left ventricular remodeling and failure after experimental myocardial infarction. *Circulation* 105: 868–873, 2002.
16. **Hironaga K, Hirooka Y, Matsuo I, Shihara M, Tagawa T, Harasawa Y, and Takeshita A.** Role of endogenous nitric oxide in the brain stem on the rapid adaptation of baroreflex. *Hypertension* 31: 27–31, 1998.
17. **Hirooka Y, Sakai K, Kishi T, and Takeshita A.** Adenovirus-mediated gene transfer into the NTS in conscious rats. A new approach to examining the central control of cardiovascular regulation. *Ann NY Acad Sci* 940: 197–205, 2001.
18. **Hirooka Y, Shigematsu H, Kishi T, Kimura Y, Ueta Y, and Takeshita A.** Reduced nitric oxide synthase in the brain stem contributes to enhanced sympathetic drive in rats with heart failure. *J Cardiovasc Pharmacol* 42, *Suppl* 1: S111–S115, 2003.
19. **Jinno S, Aika Y, Fukuda T, and Kosaka T.** Quantitative analysis of neuronal nitric oxide synthase-immunoreactive neurons in the mouse hippocampus with optical disector. *J Comp Neurol* 410: 398–412, 1999.
20. **Kishi T, Hirooka Y, Ito K, Sakai K, Shimokawa H, and Takeshita A.** Cardiovascular effects of overexpression of endothelial nitric oxide synthase in the rostral ventrolateral medulla in stroke-prone spontaneously hypertensive rats. *Hypertension* 39: 264–268, 2002.
21. **Kishi T, Hirooka Y, Kimura Y, Ito K, Shimokawa H, and Takeshita A.** Increased reactive oxygen species in rostral ventrolateral medulla contribute to neural mechanisms of hypertension in stroke-prone spontaneously hypertensive rats. *Circulation* 109: 2357–2362, 2004.
22. **Kishi T, Hirooka Y, Sakai K, Shigematsu H, Shimokawa H, and Takeshita A.** Overexpression of eNOS in the RVLM causes hypotension and bradycardia via GABA release. *Hypertension* 38: 896–901, 2001.
23. **Kumada M, Terui N, and Kuwaki T.** Arterial baroreceptor reflex: its central and peripheral neural mechanisms. *Prog Neurobiol* 35: 331–361, 1990.
24. **Lindley TE, Doobay MF, Sharma RV, and Davisson RL.** Superoxide is involved in the central nervous system activation and sympathoexcitation of myocardial infarction-induced heart failure. *Circ Res* 94: 402–409, 2004.
25. **Liu JL and Zucker IH.** Regulation of sympathetic nerve activity in heart failure: a role for nitric oxide and angiotensin II. *Circ Res* 84: 417–423, 1999.
26. **Ma R, Zucker IH, and Wang W.** Reduced NO enhances the central gain of cardiac sympathetic afferent reflex in dogs with heart failure. *Am J Physiol Heart Circ Physiol* 276: H19–H26, 1999.
27. **Mark AL.** Sympathetic dysregulation in heart failure: mechanisms and therapy. *Clin Cardiol* 18: I3–I8, 1995.
28. **Michael LH, Entman ML, Hartley CJ, Youker KA, Zhu J, Hall SR, Hawkins HK, Berens K, and Ballantyne CM.** Myocardial ischemia and reperfusion: a murine model. *Am J Physiol Heart Circ Physiol* 269: H2147–H2154, 1995.
29. **Middlekauff HR and Mark AL.** The treatment of heart failure: the role of neurohumoral activation. *Intern Med* 37: 112–122, 1998.
30. **Ooboshi H, Chu Y, Rios CD, Faraci FM, Davidson BL, and Heistad DD.** Altered vascular function after adenovirus-mediated overexpression of endothelial nitric oxide synthase. *Am J Physiol Heart Circ Physiol* 273: H265–H270, 1997.
31. **Packer M, Bristow MR, Cohn JN, Colucci WS, Fowler MB, Gilbert EM, and Shusterman NH.** The effect of carvedilol on morbidity and mortality in patients with chronic heart failure. U.S. Carvedilol Heart Failure Study Group. *N Engl J Med* 334: 1349–1355, 1996.
32. **Palkovits M.** Punch sampling biopsy technique. *Methods Enzymol* 103: 368–376, 1983.
33. **Patel KP, Zhang K, Zucker IH, and Krukoff TL.** Decreased gene expression of neuronal nitric oxide synthase in hypothalamus and brain stem of rats in heart failure. *Brain Res* 734: 109–115, 1996.
34. **Paton JF, Deuchars J, Ahmad Z, Wong LF, Murphy D, and Kasparov S.** Adenoviral vector demonstrates that angiotensin II-induced depression of the cardiac baroreflex is mediated by endothelial nitric oxide synthase in the nucleus tractus solitarii of the rat. *J Physiol* 531: 445–458, 2001.

35. **Patrick RH, Warren GY, Floyd EB, Pavel VB, and Marco RC.** *Comparative Cytoarchitectonic Atlas of the C57BL/6 and 129/Sv Mouse Brains.* Amsterdam: Elsevier Science, 2000.
36. **Patten RD, Aronovitz MJ, Deras-Mejia L, Pandian NG, Hanak GG, Smith JJ, Mendelsohn ME, and Konstam MA.** Ventricular remodeling in a mouse model of myocardial infarction. *Am J Physiol Heart Circ Physiol* 274: H1812–H1820, 1998.
37. **Phillips MI.** Antisense inhibition and adeno-associated viral vector delivery for reducing hypertension. *Hypertension* 29: 177–187, 1997.
38. **Rector TS, Olivari MT, Levine TB, Francis GS, and Cohn JN.** Predicting survival for an individual with congestive heart failure using the plasma norepinephrine concentration. *Am Heart J* 114: 148–152, 1987.
39. **Sakai K, Hirooka Y, Matsuo I, Eshima K, Shigematsu H, Shimokawa H, and Takeshita A.** Overexpression of eNOS in NTS causes hypotension and bradycardia in vivo. *Hypertension* 36: 1023–1028, 2000.
40. **Scherrer-Crosbie M, Steudel W, Ullrich R, Hunziker PR, Liel-Cohen N, Newell J, Zaroff J, Zapol WM, and Picard MH.** Echocardiographic determination of risk area size in a murine model of myocardial ischemia. *Am J Physiol Heart Circ Physiol* 277: H986–H992, 1999.
41. **Shigematsu H, Hirooka Y, Eshima K, Shihara M, Tagawa T, and Takeshita A.** Endogenous angiotensin II in the NTS contributes to sympathetic activation in rats with aortocaval shunt. *Am J Physiol Regul Integr Comp Physiol* 280: R1665–R1673, 2001.
42. **Sinnayah P, Lindley TE, Staber PD, Cassell MD, Davidson BL, and Davisson RL.** Selective gene transfer to key cardiovascular regions of the brain: comparison of two viral vector systems. *Hypertension* 39: 603–608, 2002.
43. **Suzuki M, Sasaki N, Miki T, Sakamoto N, Ohmoto-Sekine Y, Tamagawa M, Seino S, Marban E, and Nakaya H.** Role of sarcolemmal K(ATP) channels in cardioprotection against ischemia/reperfusion injury in mice. *J Clin Invest* 109: 509–516, 2002.
44. **Tai MH, Wang LL, Wu KL, and Chan JY.** Increased superoxide anion in rostral ventrolateral medulla contributes to hypertension in spontaneously hypertensive rats via interactions with nitric oxide. *Free Radic Biol Med* 38: 450–462, 2005.
45. **Tan PS, Potas JR, Killinger S, Horiuchi J, Goodchild AK, Pilowsky PM, and Dampney RA.** Angiotensin II evokes hypotension and renal sympathoinhibition from a highly restricted region in the nucleus tractus solitarii. *Brain Res* 1036: 70–76, 2005.
46. **Tseng CJ, Liu HY, Lin HC, Ger LP, Tung CS, and Yen MH.** Cardiovascular effects of nitric oxide in the brain stem nuclei of rats. *Hypertension* 27: 36–42, 1996.
47. **Vincent SR and Kimura H.** Histochemical mapping of nitric oxide synthase in the rat brain. *Neuroscience* 46: 755–784, 1992.
48. **Waagstein F, Bristow MR, Swedberg K, Camerini F, Fowler MB, Silver MA, Gilbert EM, Johnson MR, Goss FG, and Hjalmarson A.** Beneficial effects of metoprolol in idiopathic dilated cardiomyopathy. Metoprolol in Dilated Cardiomyopathy (MDC) Trial Study Group. *Lancet* 342: 1441–1446, 1993.
49. **Waki H, Kasparov S, Wong LF, Murphy D, Shimizu T, and Paton JF.** Chronic inhibition of endothelial nitric oxide synthase activity in nucleus tractus solitarii enhances baroreceptor reflex in conscious rats. *J Physiol* 546: 233–242, 2003.
50. **Wang Y, Liu XF, Cornish KG, Zucker IH, and Patel KP.** Effects of nNOS antisense in the paraventricular nucleus on blood pressure and heart rate in rats with heart failure. *Am J Physiol Heart Circ Physiol* 288: H205–H213, 2005.
51. **Wang Y, Patel KP, Cornish KG, Channon KM, and Zucker IH.** nNOS gene transfer to RVLM improves baroreflex function in rats with chronic heart failure. *Am J Physiol Heart Circ Physiol* 285: H1660–H1667, 2003.
52. **Zanzinger J, Czachurski J, and Seller H.** Inhibition of sympathetic vasoconstriction is a major principle of vasodilation by nitric oxide in vivo. *Circ Res* 75: 1073–1077, 1994.
53. **Zhang K, Li YF, and Patel KP.** Blunted nitric oxide-mediated inhibition of renal nerve discharge within PVN of rats with heart failure. *Am J Physiol Heart Circ Physiol* 281: H995–H1004, 2001.
54. **Zhang K, Zucker IH, and Patel KP.** Altered number of diaphorase (NOS) positive neurons in the hypothalamus of rats with heart failure. *Brain Res* 786: 219–225, 1998.
55. **Zucker IH, Wang W, Brandle M, Schultz HD, and Patel KP.** Neural regulation of sympathetic nerve activity in heart failure. *Prog Cardiovasc Dis* 37: 397–414, 1995.

Arteriosclerosis, Thrombosis, and Vascular Biology

JOURNAL OF THE AMERICAN HEART ASSOCIATION



**Critical Role of Mst1 in Vascular Remodeling After Injury**

Hiroki Ono, Toshihiro Ichiki, Hideki Ohtsubo, Kae Fukuyama, Ikuyo Imayama, Yasuko Hashiguchi, Junichi Sadoshima and Kenji Sunagawa

*Arterioscler. Thromb. Vasc. Biol.* 2005;25;1871-1876; originally published online Jun 16, 2005;

DOI: 10.1161/01.ATV.0000174588.50971.1a

Arteriosclerosis, Thrombosis, and Vascular Biology is published by the American Heart Association. 7272 Greenville Avenue, Dallas, TX 72514

 Print ISSN: 1079-5642. Online ISSN: 1524-4636

# Critical Role of Mst1 in Vascular Remodeling After Injury

Hiroki Ono, Toshihiro Ichiki, Hideki Ohtsubo, Kae Fukuyama, Ikuyo Imayama, Yasuko Hashiguchi, Junichi Sadoshima, Kenji Sunagawa

*Objective*—Apoptosis of vascular smooth muscle cells (VSMCs) is observed in chronic vascular lesions such as atherosclerotic plaques and is believed to contribute to the vascular remodeling process. Mst1 is a ubiquitously expressed serine/threonine kinase known to be activated in response to a wide variety of nonphysiological apoptotic stimuli. However, little is known of the physiological function of Mst1, and its role in VSMCs has never been examined.

*Methods and Results*—Treatment of VSMCs with staurosporine induced apoptosis and cleavage of Mst1, which is a marker of its activation, as well as activation of caspase 3. Adenovirus-mediated overexpression of wild-type Mst1 (AdMst1) in VSMCs increased apoptotic cells with activation of caspase 3. Mst1 was induced and activated in the balloon-injured rat carotid artery. Infection with AdMst1 in balloon-injured rat carotid artery suppressed neointimal formation compared with infection with AdLacZ. Infection with AdMst1 significantly increased the apoptotic cell number in the neointima compared with infection with AdLacZ without affecting BrdU incorporation.

*Conclusion*—Our results suggest that Mst1 plays an important role in the induction of apoptosis of VSMCs, mediating the vascular remodeling process, and may be a potential therapeutic target for vascular proliferative diseases. (*Arterioscler Thromb Vasc Biol.* **2005;25:1871-1876.**)

**Key Words:** Mst1 ■ caspase 3 ■ apoptosis ■ vascular smooth muscle cell ■ balloon injury

Apoptosis, or programmed cell death, is an active process fundamental to the development and homeostasis of multicellular organisms. Many studies have documented apoptosis of vascular smooth muscle cells (VSMCs) in human advanced atherosclerotic plaques.[1–3] Apoptosis of VSMCs has also been documented in various animal models of acute vascular injury.[4–6] These studies suggest that the balance between proliferation and apoptosis of VSMCs is one of the critical determinants of atherosclerotic lesion formation and the vascular remodeling process.[7–9] Therefore, knowledge of the key regulators of apoptosis may offer novel therapeutic targets in both the prevention and treatment of atherosclerosis.

Mammalian sterile 20-like kinase 1 (Mst1) is a ubiquitously expressed serine/threonine kinase[10] which belongs to a mammalian sterile 20-like kinase (Ste20) family.[11] Several Ste20 group kinases, including Mst1, have been reported to be involved in apoptotic response and cytoskeletal regulation.[11] Mst1 is cleaved by caspase 3 and this cleavage increases kinase activities of Mst1 by removal of the regulatory C-terminal region, which in turn activates caspase 3.[12,13] Thus, Mst1 contributes to a positive feedback loop that amplifies apoptotic responses. Most Ste20 group kinases activate the mitogen-activated protein kinase (MAPK) cascades and act as MAP kinase kinase kinase kinase (MAP4K).[11] It has been reported that Mst1 activates the p38-MAPK and the c-jun N-terminal kinase (JNK) pathways.[12] Mst1 is known to be stimulated in response to a wide variety of nonphysiological apoptotic stimuli such as staurosporine, UV, etoposide, and serum starvation;[12–16] however, few physiological activators of Mst1 are known other than engagement of Fas ligand. Recently it was reported that overexpression of Mst1 in cardiac myocytes caused dilated cardiomyopathy by stimulating apoptosis.[17] However the role of Mst1 in VSMCs or blood vessel has never been examined.

We report in the present study that overexpression of Mst1 induces VSMC apoptosis both in vitro and in vivo and suppressed neointimal formation in balloon-injured artery.

## Materials and Methods

### Materials

Dulbecco's modified Eagle's medium (DMEM) and fetal bovine serum (FBS) were purchased from GIBCO BRL. Bovine serum albumin (BSA), staurosporine, and SP600125 were purchased from Sigma Chemical Co. PD98059 was purchased from BIOMOL Research Laboratories Inc. SB203580 was a generous gift from GlaxoSmithKline (Middlesex, UK). Horseradish peroxidase conjugated secondary antibodies (anti-rabbit or anti-mouse IgG) were purchased from VECTOR Laboratories Inc. Other antibodies used in the experiments were obtained from Cell Signaling Technology. Ac-DEVD-CHO was purchased from BD Biosciences. Other chemical reagents were purchased from Wako Pure chemicals unless specifically mentioned.

Original received January 23, 2005; final version accepted June 3, 2005.

From the Department of Cardiovascular Medicine, Kyushu University Graduate School of Medical Sciences, Fukuoka, Japan: and the Cardiovascular Research Institute, University of Medicine and Dentistry of New Jersey, Newark.

Correspondence to Toshihiro Ichiki, MD, Department of Cardiovascular Medicine, Kyushu University Graduate School of Medical Sciences, 3-1-1 Maidashi, Higashi-ku, 812-8582 Fukuoka, Japan. E-mail ichiki@cardiol.med.kyushu-u.ac.jp



*Arterioscler Thromb Vasc Biol.* **is available at http://www.atvbaha.org** **DOI: 10.1161/01.ATV.0000174588.50971.1a**

### Cell Culture

VSMCs were isolated from the thoracic aorta of Sprague–Dawley rats and grown in a humidified atmosphere of 95% air/5% $CO_2$ at 37°C in DMEM. Cells were grown to confluence and growth-arrested in DMEM with 0.1% BSA for 2 days before use. Passages between 5 and 14 were used for the experiments.

### Adenovirus Vector Expressing Wild-Type Mst1 and LacZ

A recombinant adenovirus vector expressing wild-type Mst1 (AdMst1) was reported previously.[17] Confluent VSMCs were washed 2 times with PBS and incubated with AdMst1 or adenovirus vector expressing LacZ (AdLacZ) under gentle agitation for 2 hours at room temperature. Then the cells were washed 3 times, cultured in DMEM with 0.1% BSA for 2 days, and used for the experiments. Multiplicity of infection (moi) indicates the number of virus per cell added to a culture dish.

### Detection of Apoptosis

After floating cells in the supernatant were collected, attached cells were harvested through trypsinization. Collected cells were stained with Hoechst 33258. The number of apoptotic cells (cell shrinkage, chromatin condensation, and nuclear fragmentation) was counted from 500 cells under fluorescence microscopy. Cells were incubated with cold 70% ethanol and stained with propidium iodine (PI) in the presence of RNase. The fluorescence of PI from 10 000 cells was measured by flow cytometry (EPICS ALTRA MultiCOMP, Beckman Coulter) as described previously.[18]

### Western Blot Analysis

VSMCs were lysed in a sample buffer (5 mmol/L EDTA, 10 mmol/L Tris-HCl, pH 7.6, 1% Triton X-100, 50 mmol/L NaCl, 30 mmol/L sodium phosphate, 50 mmol/L NaF, 1% aprotinin, 0.5% pepstatin A, 2 mmol/L phenylmethylsulfonyl fluoride and 5 mmol/L leupeptin). Western blot analyses of Mst1, cleaved caspase 3, extracellular signal-regulated protein kinase (ERK), p38-MAPK, or JNK were performed as described previously.[19]

### Balloon Injury Model and Infection With Adenovirus

All procedures were approved by the institutional animal use and care committee and were conducted in conformity with institutional guideline. Balloon injury and infection with adenovirus were performed as described previously.[18] A male Wistar rat (300 to 350 g) was anesthetized by intraperitoneal administration of pentobarbital sodium. The left common carotid artery was denuded of the endothelium with a 2F Fogarty balloon catheter (Baxter) that was introduced through the external carotid artery. Inflation and retraction of the balloon catheter were repeated 5 times. AdMst1 or AdLacZ was introduced into the lumen, and the carotid artery was incubated for 20 minutes without blood flow. Then viral solution was removed, and blood flow was restored. $\beta$-galactosidase activity was observed in both the neointima and media in the AdLacZ-infected artery (data not shown).

### Morphometry and Immunohistochemistry

Morphometry was performed as described previously.[18] Immunohistochemistry for Mst1 was performed in frozen cross sections. In brief, after the rats were killed, the carotid artery was embedded in Optimal Cutting Temperature compound and quick-frozen in liquid nitrogen. The samples were sectioned serially at 4 $\mu$m thickness, fixed in acetone, and stained immunohistochemically with Mst1 antibody.

### Detection of Apoptosis and DNA Synthesis In Vivo

Apoptotic cells were detected by the terminal deoxynucleotidyl transferase (TdT)-mediated dUTP nick end-labeling (TUNEL) method with an apoptosis in situ detection kit (Wako Pure Chemicals) as described previously.[18] The counterstain was hematoxylin. In vivo labeling with BrdU (0.5 mg/kg), a thymidine analogue that was injected intraperitoneally 3 hours before preparation of the artery, was performed to identify replicating cells by detection of DNA synthesis. Incorporated BrdU was detected immunohistochemically with an anti-BrdU antibody (cell proliferation kit, Amersham Pharmacia Biotech). Quantitative analysis was performed from 500 cells in independent sections from each rat (n=5). The ratio of TUNEL- or BrdU-positive cells to total nucleated cells was expressed as the TUNEL index or BrdU labeling index, respectively.

### Statistical Analysis

Statistical analysis was performed with 1-way ANOVA and Fisher test if appropriate. $P<0.05$ was considered to be statistically significant. Data are shown as mean±SEM.

## Results

### Mst1 Was Activated by Apoptotic Stimuli in VSMCs

Staurosporine is a potent inducer of apoptosis in many cells. We examined whether staurosporine induced apoptosis in VSMCs. Staining with Hoechst 33258 showed that staurosporine increased the number of apoptotic cells, characterized by chromatin condensation and nuclear fragmentation (Figure 1a). Flow cytometric analysis of DNA content by PI staining showed that staurosporine increased hypodiploid cells, indicating an increase in DNA fragmentation (Figure I, available online at http://atvb.ahajournals.org). Increases in the number of hypodiploid cells by staurosporine were time- and dose-dependent (Figure I). Staurosporine induced cleavage of caspase 3 with a peak at 12 hours (Figure 1b), which indicates activation of caspase 3. These results suggest that staurosporine induced VSMC apoptosis. Mst1 cleavage was induced by staurosporine with a peak at 12 hours, which is the same peak as cleavage of caspase 3 (Figure 1b; Figure II, available online at http://atvb.ahajournals.org). Pretreatment with Ac-DEVD-CHO, a specific inhibitor of caspase 3,[20,21] inhibited Mst1 cleavage (Figure 1c). Although Ac-DEVD-CHO almost completely inhibited Mst1 activation, it partially suppressed staurosporine-induced apoptosis (Figure 1c). These data suggest that staurosporine-induced apoptosis is partially dependent on Mst1 pathway. Previous report demonstrated that $H_2O_2$ causes VSMC apoptosis[22]. $H_2O_2$ induced Mst1 cleavage with the same peak as cleavage of caspase 3 (Figure 1d). Mst1 cleavage induced by $H_2O_2$ was also inhibited by Ac-DEVD-CHO (data not shown). These data suggest that Mst1 was activated by apoptotic stimuli downstream from caspase 3 in VSMCs.

### Mst1 Induced VSMC Apoptosis

To clarify the role of Mst1 in VSMCs, we overexpressed Mst1, which induces activation of Mst1 by unknown mechanism.[12,23] Infection with AdMst1 dose-dependently increased expression of both uncleaved and cleaved Mst1 (Figure 2a). AdMst1 dose-dependently induced cleavage of caspase 3 (Figure 2a), suggesting that Mst1 activated the caspase pathway. Staining with Hoechst 33258 and PI showed that AdMst1 dose-dependently increased apoptotic cells (Figure 2b). The magnitude of the apoptotic effect of Mst1 overexpression is 29% to 44% of the apoptosis induced by staurosporine. Although infection of AdLacZ slightly increased hypodiploid cells (Figure 2b), it did not activate

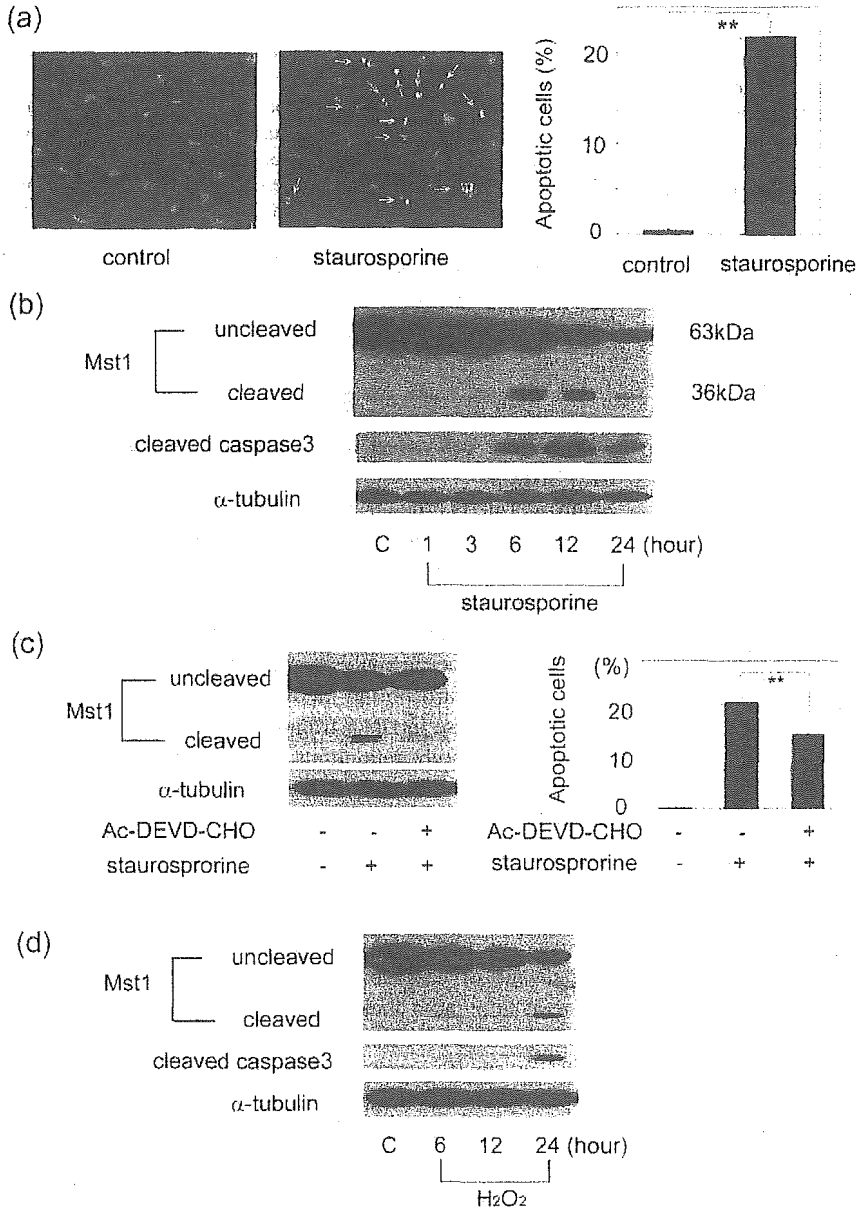


**Figure 1.** Mst1 was activated by apoptotic stimuli. a, VSMCs were stimulated with staurosporine (1 μmol/L) for 24 hours and stained with Hoechst 33258, which stains nuclei. Proportion of apoptotic cells indicated by nuclear fragmentation (indicated by arrows) is shown as bar graph (n=4). $^{**}P<0.01$ vs control. b, VSMCs were stimulated with staurosporine (1 μmol/L) for varying periods as indicated in the figure, and expression of cleaved and uncleaved Mst1 and cleaved caspase 3 was detected by Western blot analysis. Density of the specific band was scanned and quantified with an imaging analyzer. The statistical analysis of densitometric measurements of uncleaved and cleaved Mst1 expression is shown in Figure II (n=5). c, VSMCs were preincubated with Ac-DEVD-CHO (100 μmol/L) for 6 hours then stimulated with staurosporine (1 μmol/L) for 12 hours. Expression of Mst1 and cleaved caspase 3 were detected by Western blot analysis. The same results were obtained in other independent experiments and a representative autoradiogram is shown (n=4). Proportion of apoptotic cells is shown in the right panel (n=4). $^{**}P<0.01$ vs control. d, VSMCs were simulated with $H_2O_2$ (1 mmol/L) for varying periods as indicated in the figure, and expression of Mst1 and cleaved caspase 3 was detected by Western blot analysis. The same results were obtained in other independent experiments, and a representative autoradiogram is shown (n=4).

Mst1 or caspase 3 (Figure 2a) suggesting that the effect of AdLacZ may be nonspecific.

## Role of MAPKs

Many mammalian Ste20 homologs have been shown to function as MAP4K.[11] Overexpression of Mst1 induced phosphorylation of p38-MAPK and JNK; however, it did not affect phosphorylation of ERK in VSMCs (Figure IIIa, available online at http://atvb.ahajournals.org). This suggests that p38-MAPK and JNK were activated downstream from Mst1. Staurosporine induced phosphorylation of ERK, p38-MAPK, and JNK (Figure IIIb). We therefore examined which pathway was responsible for Mst1 and caspase 3 activation by staurosporine. SB203580, a p38-MAPK inhibitor, partially decreased staurosporine-induced Mst1 and caspase 3 cleavage. However, PD98059, an ERK kinase inhibitor, and SP600125, a JNK inhibitor, did not affect them (Figure IIIc). These data suggest that p38-MAPK is, at least in part, involved in staurosporine-induced Mst1 activation and apoptosis.

## Activation of Mst1 in Balloon-Injured Artery

It was reported that both proliferation and apoptosis were increased in the neointima of the balloon-injured rat carotid artery, and that the number of apoptotic cells in neointima peaked after 7 to 14 days.[24] We therefore examined whether Mst1 was activated in balloon-injured rat carotid artery. Immunohistochemistry revealed that immunoreactive Mst1 was hardly detectable in intact artery. At 14 days after balloon injury, expression of Mst1 was observed in the nuclei and, to a lesser extent, in the cytoplasm of the neointimal cells (Figure 3a), most of which are positive for α-SM actin.[18] Western blot analysis showed that expression of both uncleaved and cleaved Mst1 was significantly increased at 14 days after balloon injury, along with cleavage of caspase 3 (Figure 3b). This suggests that Mst1 was increased and

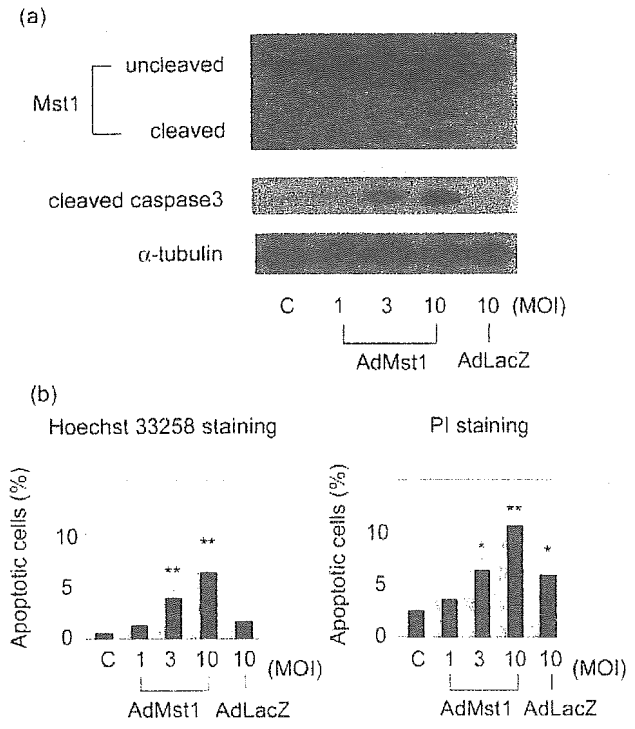


**Figure 2.** Overexpression of Mst1 induced VSMC apoptosis. a, VSMCs were infected with AdMst1 (1 to 10 moi) or AdLacZ (10 moi) for 48 hours, and expression of Mst1 and cleaved caspase 3 was detected by Western blot analysis. The same results were obtained in other independent experiments, and a representative autoradiogram is shown (n=4). b, VSMCs were infected with AdMst1 (1 to 10 moi) or AdLacZ (10 moi) for 96 hours, and apoptotic cells were detected with Hoechst 33258 and PI staining as described in the legend to Figure 1. Proportion of apoptotic cells is shown as a bar graph (n=4). $^{**}P<0.01$ vs control and AdLacZ. $^{*}P<0.01$ vs control

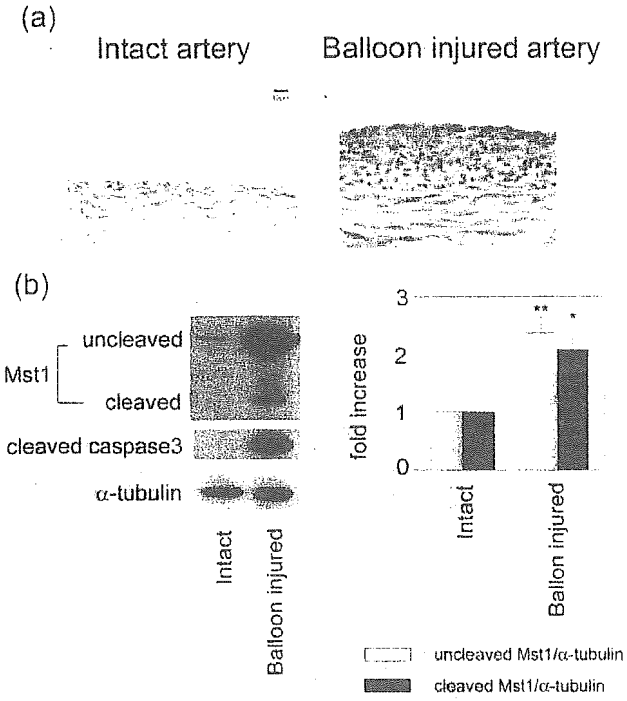


**Figure 3.** Expression of Mst1 in balloon-injured artery. a, Representative microphotographs of immunohistochemistry for Mst1 in intact and injured carotid artery at 14 days after injury (n=5). b, Western blot analysis of Mst1 and cleaved caspase 3 in balloon-injured rat carotid artery at 14 days after injury is shown. The ratio of uncleaved Mst1 (white bars) or cleaved Mst1 (black bars) to α-tubulin is shown in the right panel (n=6). The values are expressed as mean±SEM, $^{**}P<0.01$ vs control, $^{*}P<0.05$ vs control.

activated in the process of vascular remodeling after balloon injury. We overexpressed Mst1 in balloon-injured artery by infection with AdMst1. Infection with AdMst1 suppressed neointimal formation (I/M ratio) compared with infection with AdLacZ 14 days after balloon injury (Figure 4a and 4b). The intimal area was suppressed in AdMst1-infected artery compared with AdLacZ-infected one without affecting the medial area (Figure 4b). It was previously reported that the TUNEL index peaked after 7 to 14 days of vascular injury, and the BrdU labeling index peaked after 7 days.[24] TUNEL index in the neointima of AdMst1-infected arteries was significantly increased compared with that of AdLacZ-infected arteries, whereas AdMst1 did not affect the TUNEL index in medial cells at 14 days after balloon injury (Figure 4c). Infection with AdMst1 did not affect the BrdU labeling index in either the neointima or media at 7 days after injury (Figure 4c).

## Discussion

In the present study, we showed that overexpression of Mst1 induced VSMC apoptosis in vitro and in vivo and suppressed neointimal formation in balloon-injured artery. This is the first report examining the function of Mst1 in VSMCs and in balloon-injured artery. A recent study reported that cardiac-specific overexpression of Mst1 causes dilated cardiomyopathy,[17] suggesting that apoptosis of cardiac myocytes impairs cardiac function. However, overexpression of Mst1 in injured artery has antiproliferative effect by stimulating apoptosis, which may be used as a therapeutic tool for vascular proliferative lesion such as in-stent restenosis.

Numerous animal models of acute balloon injury of artery have documented apoptotic VSMC death. Several studies demonstrated that balloon injury of vessels induces two waves of VSMC apoptosis. The first wave of apoptosis occurred in the media within hours of the injury.[5] The second wave occurs at much later times after injury (days to weeks). VSMC accumulation in the neointima of injured rat carotid arteries reached a maximal level at 2 weeks after injury; however, cellular proliferation continues for up to 12 weeks.[25] Therefore, it is thought that this second wave of apoptosis limits lesion growth. The rates of neointimal VSMC death and proliferation are in equilibrium at 2 weeks, thereby preventing further increase in lesion size. Expression of both the uncleaved and cleaved forms of Mst1 was increased after balloon injury. Upregulation of uncleaved and cleaved Mst1 indicated that Mst1 kinase activity was increased and may contribute to the delayed enhancement of apoptosis in the neointimal formation. Although genotoxic agents are known to activate Mst1, this is the first report showing that clinically relevant stimuli such as balloon injury activate Mst1 in blood vessel. An in vitro study suggested that reactive oxygen

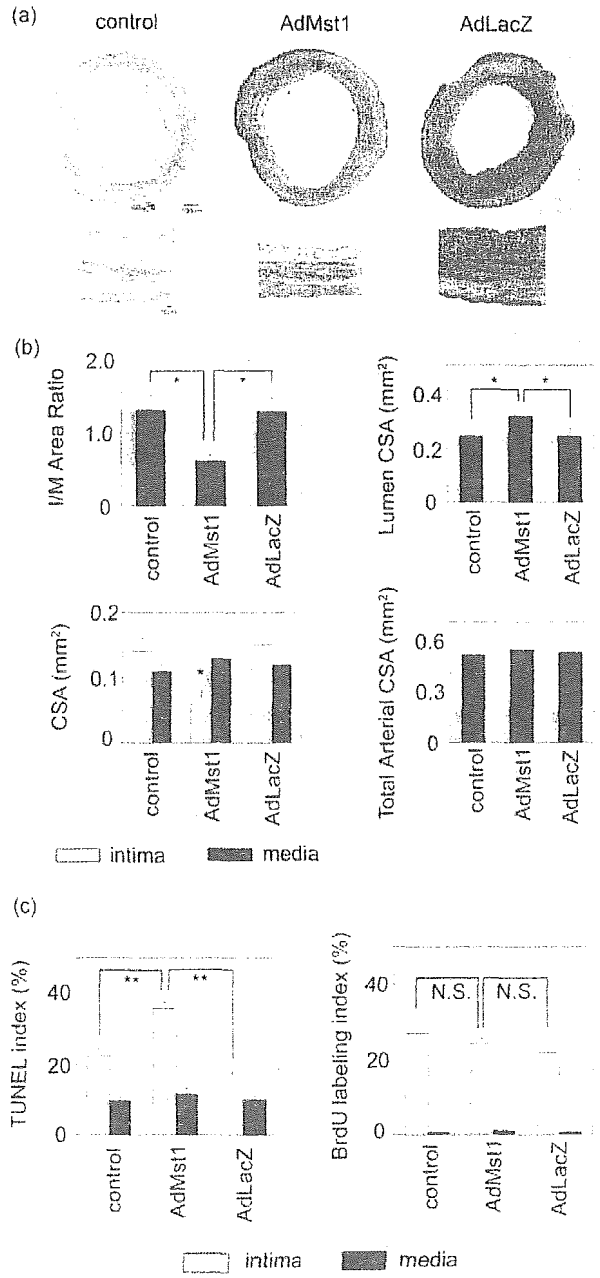


**Figure 4.** Overexpression of Mst1 in balloon-injured artery. a, Representative microphotographs of hematoxylin-eosin staining of cross sections of carotid arteries 14 days after balloon injury. The same results were obtained in other independent experiments (n=5). b, The intima/media area ratio (I/M ratio) and cross-section area (CSA) of intima, media, lumen, and total artery in injured artery are shown as bar graphs (n=5). The values are expressed as mean±SEM, *$P<0.05$ vs control or AdLacZ. c, TUNEL or BrdU labeling were performed in cross sections of carotid arteries 14 or 7 days after balloon injury. TUNEL index of intima (black bars) or media (white bars) is indicated in a left bar graph (n=5). BrdU labeling index of intima (white bars) or media (black bars) is indicated in a right bar graph (n=5). The values are expressed as mean±SEM, **$P<0.01$ vs control or AdLacZ; N.S.=not significant.

species may be involved in the activation of Mst1 in injured artery. Regulation of Mst1 expression has not been examined in detail, and the mechanism of Mst1 upregulation and activation in injured rat carotid artery is not clear at this point. Further studies are necessary to determine the mechanism of Mst1 upregulation and activation in injured blood vessel.

We showed in the present study that Mst1 was activated in apoptotic response by staurosporine and that overexpression of Mst1 induced apoptosis in VSMCs. Several studies have demonstrated that Mst1 is necessary for the induction of apoptosis. A kinase-negative mutant of Mst1 in which Lys-59 is changed to Arg inhibited staurosporine-induced chromatin condensation[26] and chelerythrine-induced DNA fragmentation.[17] Suppression of endogenous Mst1 by cardiac-specific overexpression of the kinase-negative mutant of Mst1 in transgenic mice prevented myocyte death induced by ischemia/reperfusion.[17] These data suggest that Mst1 plays an essential role in mediating apoptotic response, which may be true in blood vessel as well.

Most Ste20 group kinases act as MAP4K, and it has been reported that Mst1 activates the p38-MAPK and JNK pathways.[12] Mst1 has been shown to function upstream from MEKK1 and MKK7 in the JNK pathway[12,27] and upstream from MKK6 in the p38-MAPK pathway.[12] These results are consistent with Mst1 function as a MAP4K. However, there are conflicting evidences as to which pathway mediates apoptosis downstream of Mst1. Graves et al reported that the p38-MAPK pathway may mediate Mst1-induced apoptosis because SB203580 inhibited Mst1-induced morphological changes in 293T cells.[12] Another group reported that a dominant-negative mutant of JNK inhibited Mst1-induced morphological changes as well as caspase activation, while a dominant-negative p38-MAPK did not.[23] In VSMCs, p38-MAPK and JNK were both activated downstream of Mst1, and a p38-MAPK inhibitor partially inhibited staurosporine-induced Mst1 and caspase 3 cleavage. These data suggest that p38-MAPK, at least in part, mediates apoptotic response through Mst1 in VSMCs. p38-MAPK is activated both upstream and downstream of Mst1 and may be involved in the positive feedback loop formed by Mst1 and caspase 3. However, the effect of SB203580 was partial, suggesting that some pathway other than p38-MAPK is also involved in apoptosis induced by staurosporine, thus requiring further investigation.

Recently, it has been reported that Hippo, the Drosophila homologue of Mst1/2, promotes apoptosis and proper termination of cell proliferation during development, together with Salvador, the Drosophila homologue of hWW45, and Warts, the Drosophila homologue of large tumor suppressor (LATS), in a signal module complex.[28,29] Although mutations in the hWW45 gene have been reported in three cancer cell lines,[30] its function has not been examined in detail. The roles of hWW45 or LATS in VSMCs and the relationship between Mst1/2 and hWW45 or LATS in blood vessel require further investigation.

Many environmental factors and endogenous proteins regulate the struggle between apoptosis and proliferation in atherosclerotic lesion. Several reports suggest that apoptosis in atherosclerotic plaque may decrease its stability and induce plaque rupture.[31,32] A recent report showed that proapoptotic genes were highly expressed in atherosclerotic plaques from patients with acute coronary syndrome compared with those

from patients with stable angina.[33] However, induction of apoptosis may be useful for the treatment of in-stent restenosis that is rich in cellular component such as VSMCs.[34,35]

The data presented in the present study suggest that Mst1 plays a critical role in the vascular remodeling process and could be a therapeutic target for prevention of restenosis after vascular injury.

## Acknowledgments

This study was supported in part by grants from Takeda Science Foundation and a Grant-in-aid for Scientific Research from the Ministry of Education, Culture, Sports, Science, and Technology of Japan (17590742). We thank Daniela Zablocki for critical reading of the manuscript.

## References

1. Isner JM, Kearney M, Bortman S, Passeri J. Apoptosis in human atherosclerosis and restenosis. *Circulation*. 1995;91:2703–2711.
2. Bennett MR, Evan GI, Schwartz SM. Apoptosis of human vascular smooth muscle cells derived from normal vessels and coronary atherosclerotic plaques. *J Clin Invest*. 1995;95:2266–2274.
3. Geng YJ, Libby P. Evidence for apoptosis in advanced human atheroma. Colocalization with interleukin-1 beta-converting enzyme. *Am J Pathol*. 1995;147:251–266.
4. Bochaton-Piallat ML, Gabbiani F, Redard M, Desmouliere A, Gabbiani G. Apoptosis participates in cellularity regulation during rat aortic intimal thickening. *Am J Pathol*. 1995;146:1059–1064.
5. Perlman H, Maillard L, Krasinski K, Walsh K. Evidence for the rapid onset of apoptosis in medial smooth muscle cells after balloon injury. *Circulation*. 1997;95:981–987.
6. Malik N, Francis SE, Holt CM, Gunn J, Thomas GL, Shepherd L, Chamberlain J, Newman CM, Cumberland DC, Crossman DC. Apoptosis and cell proliferation after porcine coronary angioplasty. *Circulation*. 1998;98:1657–1665.
7. Bennett MR, Boyle JJ. Apoptosis of vascular smooth muscle cells in atherosclerosis. *Atherosclerosis*. 1998;138:3–9.
8. Walsh K, Smith RC, Kim HS. Vascular cell apoptosis in remodeling, restenosis, and plaque rupture. *Circ Res*. 2000;87:184–188.
9. Geng YJ, Libby P. Progression of atheroma: a struggle between death and procreation. *Arterioscler Thromb Vasc Biol*. 2002;22:1370–1380.
10. Creasy CL, Chernoff J. Cloning and characterization of a human protein kinase with homology to Ste20. *J Biol Chem*. 1995;270:21695–21700.
11. Dan I, Watanabe NM, Kusumi A. The Ste20 group kinases as regulators of MAP kinase cascades. *Trends Cell Biol*. 2001;11:220–230.
12. Graves JD, Gotoh Y, Draves KE, Ambrose D, Han DK, Wright M, Chernoff J, Clark EA, Krebs EG. Caspase-mediated activation and induction of apoptosis by the mammalian Ste20-like kinase Mst1. *Embo J*. 1998;17:2224–2234.
13. Lee KK, Murakawa M, Nishida E, Tsubuki S, Kawashima S, Sakamaki K, Yonehara S. Proteolytic activation of MST/Krs, STE20-related protein kinase, by caspase during apoptosis. *Oncogene*. 1998;16:3029–3037.
14. Lu ML, Sato M, Cao B, Richie JP. UV irradiation-induced apoptosis leads to activation of a 36-kDa myelin basic protein kinase in HL-60 cells. *Proc Natl Acad Sci U S A*. 1996;93:8977–8982.
15. Cheung WL, Ajiro K, Samejima K, Kloc M, Cheung P, Mizzen CA, Beeser A, Etkin LD, Chernoff J, Earnshaw WC, Allis CD. Apoptotic phosphorylation of histone H2B is mediated by mammalian sterile twenty kinase. *Cell*. 2003;113:507–517.
16. Reszka AA, Halasy-Nagy JM, Masarachia PJ, Rodan GA. Bisphosphonates act directly on the osteoclast to induce caspase cleavage of mst1 kinase during apoptosis. A link between inhibition of the mevalonate pathway and regulation of an apoptosis-promoting kinase. *J Biol Chem*. 1999;274:34967–34973.
17. Yamamoto S, Yang G, Zablocki D, Liu J, Hong C, Kim SJ, Soler S, Odashima M, Thaisz J, Yehia G, Molina CA, Yatani A, Vatner DE, Vatner SF, Sadoshima J. Activation of Mst1 causes dilated cardiomyopathy by stimulating apoptosis without compensatory ventricular myocyte hypertrophy. *J Clin Invest*. 2003;111:1463–1474.
18. Tokunou T, Shibata R, Kai H, Ichiki T, Morisaki T, Fukuyama K, Ono H, Iino N, Masuda S, Shimokawa H, Egashira K, Imaizumi T, Takeshita A. Apoptosis induced by inhibition of cyclic AMP response element-binding protein in vascular smooth muscle cells. *Circulation*. 2003;108:1246–1252.
19. Tokunou T, Ichiki T, Takeda K, Funakoshi Y, Iino N, Shimokawa H, Egashira K, Takeshita A. Thrombin induces interleukin-6 expression through the cAMP response element in vascular smooth muscle cells. *Arterioscler Thromb Vasc Biol*. 2001;21:1759–1763.
20. Nicholson DW, Ali A, Thornberry NA, Vaillancourt JP, Ding CK, Gallant M, Gareau Y, Griffin PR, Labelle M, Lazebnik YA, Munday NA, Raju SM, Smulson ME, Yamin TT, Yu VL, Miller DK. Identification and inhibition of the ICE/CED-3 protease necessary for mammalian apoptosis. *Nature*. 1995;376:37–43.
21. Talanian RV, Quinlan C, Trautz S, Hackett MC, Mankovich JA, Banach D, Ghayur T, Brady KD, Wong WW. Substrate specificities of caspase family proteases. *J Biol Chem*. 1997;272:9677–9682.
22. Li PF, Maasch C, Haller H, Dietz R, von Harsdorf R. Requirement for protein kinase C in reactive oxygen species-induced apoptosis of vascular smooth muscle cells. *Circulation*. 1999;100:967–973.
23. Ura S, Masuyama N, Graves JD, Gotoh Y. MST1-JNK promotes apoptosis via caspase-dependent and independent pathways. *Genes Cells*. 2001;6:519–530.
24. Shibata R, Kai H, Seki Y, Kato S, Morimatsu M, Kaibuchi K, Imaizumi T. Role of Rho-associated kinase in neointima formation after vascular injury. *Circulation*. 2001;103:284–289.
25. Clowes AW, Reidy MA, Clowes MM. Kinetics of cellular proliferation after arterial injury. I. Smooth muscle growth in the absence of endothelium. *Lab Invest*. 1983;49:327–333.
26. Ura S, Masuyama N, Graves JD, Gotoh Y. Caspase cleavage of MST1 promotes nuclear translocation and chromatin condensation. *Proc Natl Acad Sci U S A*. 2001;98:10148–10153.
27. Graves JD, Draves KE, Gotoh Y, Krebs EG, Clark EA. Both phosphorylation and caspase-mediated cleavage contribute to regulation of the Ste20-like protein kinase Mst1 during CD95/Fas-induced apoptosis. *J Biol Chem*. 2001;276:14909–14915.
28. Udan RS, Kango-Singh M, Nolo R, Tao C, Halder G. Hippo promotes proliferation arrest and apoptosis in the Salvador/Warts pathway. *Nat Cell Biol*. 2003;5:914–920.
29. Pantalacci S, Tapon N, Leopold P. The Salvador partner Hippo promotes apoptosis and cell-cycle exit in Drosophila. *Nat Cell Biol*. 2003;5:921–927.
30. Tapon N, Harvey KF, Bell DW, Wahrer DC, Schiripo TA, Haber DA, Hariharan IK. salvador Promotes both cell cycle exit and apoptosis in Drosophila and is mutated in human cancer cell lines. *Cell*. 2002;110:467–478.
31. Bjorkerud S, Bjorkerud B. Apoptosis is abundant in human atherosclerotic lesions, especially in inflammatory cells (macrophages and T cells), and may contribute to the accumulation of gruel and plaque instability. *Am J Pathol*. 1996;149:367–380.
32. Libby P. Molecular bases of the acute coronary syndromes. *Circulation*. 1995;91:2844–2850.
33. Rossi ML, Marziliano N, Merlini PA, Bramucci E, Canosi U, Belli G, Parenti DZ, Mannucci PM, Ardissino D. Different quantitative apoptotic traits in coronary atherosclerotic plaques from patients with stable angina pectoris and acute coronary syndromes. *Circulation*. 2004;110:1767–1773.
34. Farb A, Sangiorgi G, Carter AJ, Walley VM, Edwards WD, Schwartz RS, Virmani R. Pathology of acute and chronic coronary stenting in humans. *Circulation*. 1999;99:44–52.
35. Komatsu R, Ueda M, Naruko T, Kojima A, Becker AE. Neointimal tissue response at sites of coronary stenting in humans: macroscopic, histological, and immunohistochemical analyses. *Circulation*. 1998;98:224–233.

# Selective disruption of MMP-2 gene exacerbates myocardial inflammation and dysfunction in mice with cytokine-induced cardiomyopathy

**Hidenori Matsusaka, Masaki Ikeuchi, Shouji Matsushima, Tomomi Ide, Toru Kubota, Arthur M. Feldman, Akira Takeshita, Kenji Sunagawa and Hiroyuki Tsutsui**

*AJP - Heart* 289:1858-1864, 2005. First published Jun 3, 2005; doi:10.1152/ajpheart.00216.2005

*Am J Physiol Heart Circ Physiol* 289: H1858–H1864, 2005.
First published June 3, 2005; doi:10.1152/ajpheart.00216.2005.

# Selective disruption of MMP-2 gene exacerbates myocardial inflammation and dysfunction in mice with cytokine-induced cardiomyopathy

**Hidenori Matsusaka,[1] Masaki Ikeuchi,[1] Shouji Matsushima,[1] Tomomi Ide,[1] Toru Kubota,[1] Arthur M. Feldman,[2] Akira Takeshita,[1] Kenji Sunagawa,[1] and Hiroyuki Tsutsui[3]**

[1]*Department of Cardiovascular Medicine, Kyushu University Graduate School of Medical Sciences, Fukuoka;* [3]*Department of Cardiovascular Medicine, Hokkaido University Graduate School of Medicine, Sapporo, Japan; and* [2]*Department of Medicine, Jefferson Medical College, Philadelphia, Pennsylvania*

Submitted 7 March 2005; accepted in final form 23 May 2005

**Matsusaka, Hidenori, Masaki Ikeuchi, Shouji Matsushima, Tomomi Ide, Toru Kubota, Arthur M. Feldman, Akira Takeshita, Kenji Sunagawa, and Hiroyuki Tsutsui.** Selective disruption of MMP-2 gene exacerbates myocardial inflammation and dysfunction in mice with cytokine-induced cardiomyopathy. *Am J Physiol Heart Circ Physiol* 289: H1858–H1864, 2005. First published June 3, 2005; doi:10.1152/ajpheart.00216.2005.—Tumor necrosis factor-α (TNF-α) plays a pathophysiological role in the development and progression of heart failure. Matrix metalloproteinase (MMP)-2 is involved in extracellular matrix remodeling. Recent evidence suggests a protective role for this protease against tissue inflammation. Although MMP-2 is upregulated in the failing heart, little is known about its pathophysiological role. We thus hypothesized that ablation of the MMP-2 gene could affect cardiac remodeling and failure in TNF-α-induced cardiomyopathy. We crossed transgenic mice with cardiac-specific overexpression of TNF-α (TG) with MMP-2 knockout (KO) mice. Four groups of male and female mice were studied: wild-type (WT) with wild MMP-2 (WT/MMP$^{+/+}$), WT with MMP-2 KO (WT/MMP$^{-/-}$), TNF-α TG with wild MMP-2 (TG/MMP$^{+/+}$), and TG with MMP-2 KO (TG/MMP$^{-/-}$). The upregulation of MMP-2 zymographic activity in TG/MMP$^{+/+}$ mice was completely abolished in TG/MMP$^{-/-}$ mice, and other MMPs and tissue inhibitors of metalloproteinase were comparable between groups. Survival was shorter for male TG/MMP$^{-/-}$ than TG/MMP$^{+/+}$ mice. Female TG/MMP$^{-/-}$ mice were more severely affected than TG/MMP$^{+/+}$ mice with diminished cardiac function. Myocardial TNF-α and other proinflammatory cytokines were increased in TG/MMP$^{+/+}$ mice, and this increase was similarly observed in TG/MMP$^{-/-}$ mice. The extent of myocardial infiltrating cells including macrophages was greater in TG/MMP$^{-/-}$ than in TG/MMP$^{+/+}$ mice. Selective ablation of the MMP-2 gene reduces survival and exacerbates cardiac failure in association with the increased level of myocardial inflammation. MMP-2 may play a cardioprotective role in the pathogenesis of cytokine-induced cardiomyopathy.

metalloproteinases; heart failure; tumor necrosis factor

THE DYNAMIC SYNTHESIS and breakdown of extracellular matrix (ECM) proteins play an important role in myocardial remodeling and failure. In particular, increased expression and activation of matrix metalloproteinases (MMPs) have been implicated in heart failure (4, 8, 20, 23, 26, 27). The activity of MMPs is controlled by transcription, activation of the latent proenzymes, and inhibition of MMPs by tissue inhibitors of MMPs (TIMPs). Although transcriptional regulation is essential for MMP production, activation of latent enzymes by proteolytic cleavage is required for matrix degradation. In addition, TIMPs modulate ECM deposition through inhibition of activated MMPs. Together, activation of latent MMP and inhibition of MMPs by TIMPs contribute to myocardial remodeling and failure. Among the known MMPs, MMP-2 is ubiquitously distributed in cardiac myocytes and fibroblasts (2) and has been shown to be upregulated in heart failure (1, 8). Recent studies have shown that MMP-2 has diverse cellular function, such as attenuation of the tissue inflammatory response, independent of its action on the ECM (3, 13, 29). Therefore, the ultimate effects of MMPs may include modulation of ECM proteins, as well as modification of cellular functions, including cell migration.

Myocardial production of proinflammatory cytokines, including tumor necrosis factor-α (TNF-α), plays an important role in the pathogenesis of heart failure (5, 22). Transgenic (TG) mice that overexpress TNF-α specifically in the heart developed myocardial inflammation, with premature death from heart failure in association with ECM remodeling (16, 17). Activation of MMPs, i.e., MMP-2 and MMP-9, has been demonstrated in this model (17, 18). Furthermore, expression of MMP-2 can be regulated by the inflammatory cytokines (19). Therefore, MMP-2 could influence the progression of inflammation by affecting the function of mediators such as cytokines/chemokines and could play an important role in myocardial remodeling. In the present study, we evaluated the effects of a targeted deletion of the MMP-2 gene on cardiac structural and functional alterations in this type of heart failure. To ensure selective and long-term complete inhibition of MMP-2, we crossed TNF-α TG mice with MMP-2 knockout (KO) mice (8, 12). The most effective way to evaluate the contribution of a specific MMP and obtain direct evidence for a role of MMP is through gene manipulation instead of an MMP inhibitor.

## MATERIALS AND METHODS

*Animal model.* We used TG mice with cardiac-specific overexpression of TNF-α, which have been well characterized as a model of cytokine-induced cardiomyopathy (16). To ensure complete inhibition of MMP-2 activity, we crossed TG mice with MMP-2 KO (MMP$^{-/-}$) mice. There were no detectable differences in cardiac size and structure between MMP$^{-/-}$ and MMP$^{+/+}$ mice either macroscopically or microscopically (8). The original breeding pairs used to develop the mice for this study were obtained from Dr. Shigeyoshi Itohara (Laboratory for Behavioral Genetics, RIKEN). Because

Address for reprint requests and other correspondence: H. Tsutsui, Dept. of Cardiovascular Medicine, Hokkaido Univ. Graduate School of Medicine, Kita-15, Nishi-7, Kita-ku, Sapporo 060-8638, Japan (E-mail: htsutsui@med.hokudai.ac.jp).

The costs of publication of this article were defrayed in part by the payment of page charges. The article must therefore be hereby marked "*advertisement*" in accordance with 18 U.S.C. Section 1734 solely to indicate this fact.

TNF-α TG (FVB) and MMP-2 KO (C57BL/6J) mice arise from different genetic backgrounds, we generated all mice as mixed genetic background (1:1 ratio of C57BL/6J to FVB) to minimize genetic heterogeneity of the mice, as described previously (6, 10). Briefly, mating male TG mice with female $MMP^{-/-}$ mice yielded TG or wild-type (WT) mice with $MMP^{+/-}$ (F1). Then we mated TG and WT mice with $MMP^{+/-}$ mice to obtain TG or WT mice with $MMP^{+/+}$, $MMP^{+/-}$, and $MMP^{-/-}$ (F2). To minimize the effect of genetic background, littermates were studied in each analysis. The study was approved by our Institutional Animal Research Committee and conformed to the animal care guidelines of the American Physiological Society.

*MMPs and TIMPs.* Myocardial MMP levels, including MMP-2 and MMP-9, were determined in the left ventricle (LV) from 12-wk-old female mice by gelatin zymography (8). The LV myocardial samples were homogenized (~30-s bursts) in 1 ml of an ice-cold extraction buffer containing cacodylic acid (10 mmol/l), NaCl (0.15 mol/l), $ZnCl_2$ (20 mmol/l), $NaN_2$ (1.5 mmol/l), and 0.01% Triton X-100 (pH 5.0). The homogenate was then centrifuged (4°C, 10 min, 10,000 *g*), and the supernatant was decanted and saved on ice. The pH levels of the samples were adjusted to 7.5 with Tris (1 mol/l). The final protein concentration of the myocardial extracts was determined using a standardized colorimetric assay. The extracted samples were aliquoted and stored at −80°C until the time of assay. The myocardial extracts were then directly loaded onto electrophoretic gels (SDS-PAGE) containing 1 mg/ml gelatin under nonreducing conditions. The myocardial extracts at a final protein content of 5 μg were loaded onto the gels using a 3:1 sample buffer (10% SDS, 4% sucrose, 0.25 mol/l Tris·Cl, and 0.1% bromphenol blue, pH 6.8). The gels were run at 15 mA/gel through the stacking phase (4%) and at 20 mA/gel for the separating phase (10%), while the running buffer temperature was maintained at 4°C. After SDS-PAGE, the gels were washed twice in 2.5% Triton X-100 for 30 min each, rinsed in water, and incubated for 24 h in a substrate buffer at 37°C (50 mmol/l Tris·HCl, 5 mmol/l, $CaCl_2$, and 0.02% $NaN_3$, pH 7.5). After incubation, the gels were stained with Coomassie brilliant blue R-250. The zymograms were digitized, and the size-fractionated bands, which indicated MMP proteolytic levels, were measured by integrated optical density in a rectangular region of interest.

The mRNA levels of myocardial MMPs, including MMP-1, MMP-2, MMP-3, MMP-8, and MMP-9, as well as TIMPs, including TIMP-1, TIMP-2, TIMP-3, and TIMP-4, were determined by multiprobe ribonuclease protection assay (RiboQuant, PharMingen). Each value was normalized to that of glyceraldehyde-3-phosphate dehydrogenase (GAPDH) in each template set as an internal control and then calculated as a ratio to $WT/MMP^{+/+}$.

*Survival.* Survival was analyzed in male and female $WT/MMP^{+/+}$, $WT/MMP^{-/-}$, $TG/MMP^{+/+}$, and $TG/MMP^{-/-}$ mice. During the study period, the cages were inspected daily to identify any deceased animals. All deceased mice were examined for the presence of pleural effusion (serous fluid within the chest wall cavity) in the postmortem examination. Because most of the male TG mice died earlier, we used 12-wk-old female mice for the subsequent analyses.

*Echocardiographic and hemodynamic measurements.* Echocardiographic studies were performed under light anesthesia with tribromoethanol-amylene hydrate (Avertin, 2.5% wt/vol, 8 μl/g ip) and spontaneous respiration as described previously (24). A two-dimensional parasternal short-axis view of the LV was obtained at the level of the papillary muscles. In general, the best views were obtained with the transducer lightly applied to the midportion of the upper left anterior chest wall. The transducer was then gently moved cephalad or caudad and angulated until desirable images were obtained. After confirmation that the imaging was on axis (on the basis of roundness of the LV cavity), two-dimensional targeted M-mode traces were recorded at a paper speed of 50 mm/s. Then a 1.4-Fr micromanometer-tipped catheter (Millar) was inserted into the right carotid artery and advanced into the LV to measure LV pressures. Our previous validation study showed that intra- and interobserver variabilities of our echocardiographic measurements for LV cavity dimensions and fractional shortening were small and that measurements made in the same animals on separate days were highly reproducible (24).

*Histopathology.* After in vivo echocardiographic and hemodynamic studies, the heart was excised and dissected into right ventricle and LV, including the septum. From the mid-LV transverse sections, 5-μm sections were cut and stained with hematoxylin and eosin and Masson's trichrome for determination of myocyte cross-sectional area and collagen volume fraction. They were stained also with picrosirius red for visualization of the interstitial collagen fibers.

Myocardial infiltration was quantified in hematoxylin-and-eosin-stained sections by determination of nuclear density (nuclei/$mm^2$) according to methods described previously (15, 21). Because it is difficult to differentiate inflammatory cells from myocytes and/or fibroblasts, all nuclei were included. In each animal, five independent high-power fields were analyzed. To further determine the number of macrophages, an immunohistochemical analysis using a specific antibody against mouse Mac-3 (BD Pharmingen) was performed.

*Cytokine gene expression.* To determine the myocardial gene expression of TNF-α as well as other proinflammatory cytokines, including regulated on activation, normal T cell expressed and secreted (RANTES), interleukin (IL)-6, IL-1β, transforming growth factor (TGF)-β, and monocyte chemoattractant protein (MCP)-1, ribonuclease protection assay was performed with 5 μg of total RNA isolated from LV tissue samples according to methods described previously (11).

*Plasma cytokine and MMP levels.* Plasma levels of TNF-α, as well as other cytokines, were measured with commercially available ELISA kits for mouse TNF-α, IL-6, IL-1β, and MCP-1 (Quantikine, R & D Systems). Plasma MMP-2 was also measured with commercially available ELISA kits (Quantikine). All assays were done in duplicate. Results were analyzed spectrophotometrically at a wavelength of 450 nm with a microtiter plate reader.

*Statistical analysis.* Values are means ± SE. A survival analysis was performed by the Kaplan-Meier method, and between-group difference in survival was tested by the log-rank test. Between-group comparisons of the means were performed by one-way ANOVA followed by *t*-tests. Bonferroni's correction was done for multiple comparisons of the means.

## RESULTS

*MMPs and TIMPs.* Zymographic MMP-2 levels increased in TNF-α $TG/MMP^{+/+}$ compared with $WT/MMP^{+/+}$ mice (Fig. 1). As expected, MMP-2 activity was not detected in $WT/MMP^{-/-}$ and $TG/MMP^{-/-}$ mice. Importantly, the MMP-9 zymographic levels, even though they were faint in $WT/MMP^{+/+}$ mice, did not increase in $WT/MMP^{-/-}$ mice. They significantly increased in the TNF-α TG groups; however, no difference was seen between $TG/MMP^{+/+}$ and $TG/MMP^{-/-}$ mice.

Again, the MMP-2 mRNA levels significantly increased in TNF-α $TG/MMP^{+/+}$ compared with $WT/MMP^{+/+}$ mice (Fig. 2). This increase was completely prevented in $TG/MMP^{-/-}$ mice. The MMP-9 mRNA levels also increased in the TNF-α TG groups; however, no difference was seen between $TG/MMP^{+/+}$ and $TG/MMP^{-/-}$ mice. These results were consistent with those observed in gelatin zymography (Fig. 1). Other MMPs, including MMP-1, MMP-3, and MMP-8, were not altered in these mice (Fig. 2). The changes in TIMPs (TIMP-1, TIMP-2, TIMP-3, and TIMP-4) were comparable between $TG/MMP^{+/+}$ and $TG/MMP^{-/-}$ mice.

*Survival.* Survival rate was shorter for male $TG/MMP^{-/-}$ than $TG/MMP^{+/+}$ mice (Fig. 3). Although MMP-2 gene ab-

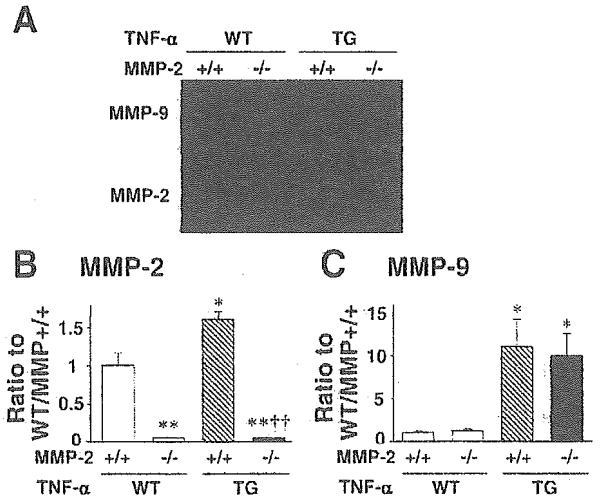


Fig. 1. *A*: representative gelatin zymography of left ventricle (LV) from wild-type (WT) mice with wild matrix metalloproteinase-2 (WT/MMP$^{+/+}$), WT mice with MMP-2 knockout (KO) (WT/MMP$^{-/-}$), TNF-α transgenic (TG) mice with MMP-2 (TG/MMP$^{+/+}$), and TNF-α TG mice with MMP-2 KO (TG/MMP$^{-/-}$). *B* and *C*: densitometric analysis of MMP-2 and MMP-9 zymographic activity ($n$ = 3/group). Samples from WT/MMP$^{+/+}$ mice were run concurrently on the same gel. Values are means ± SE. *$P$ < 0.05; **$P$ < 0.01 vs. WT/MMP$^{+/+}$. ††$P$ < 0.01 vs. TG/MMP$^{+/+}$.

lation was also observed in female mice, it has less effect on survival. These observations of gender differences in survival were consistent with results from a previous study (14), which demonstrated that such gender differences might be due to higher expression of TNF-α receptors in the myocardium of male TG mice, because the extent of myocardial expression of TNF-α was comparable in both genders (14). All the TG mice that died spontaneously developed cardiac dilatation and pleural effusion, suggesting that they died of heart failure. Because most of the male TG mice died earlier, we used surviving 12-wk-old female mice for the subsequent analyses.

*Echocardiography and hemodynamics.* The echocardiographic and hemodynamic data of the surviving 12-wk-old

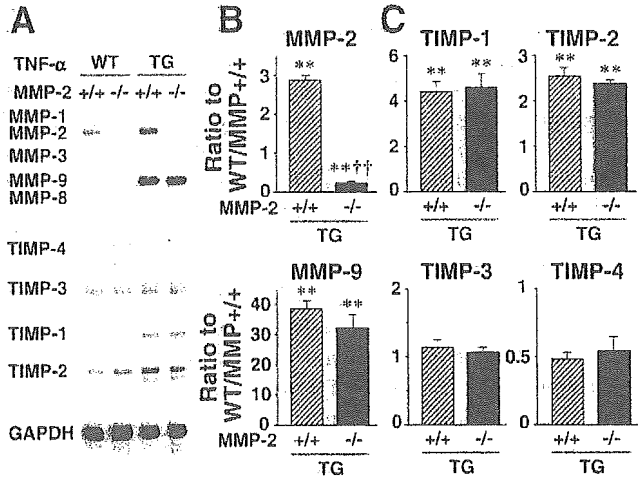


Fig. 2. *A*: representative image of myocardial gene expression of MMPs and tissue inhibitors of MMPs (TIMPs). *B* and *C*: densitometric analysis of MMP and TIMP gene expression in TG/MMP$^{+/+}$ ($n$ = 7) and TG/MMP$^{-/-}$ ($n$ = 7) mice. Each value was normalized to that of GAPDH in each template set as an internal control and expressed as ratio to WT/MMP$^{+/+}$ ($n$ = 6). Values are means ± SE. **$P$ < 0.01 vs. WT/MMP$^{+/+}$. ††$P$ < 0.01 vs. TG/MMP$^{+/+}$.

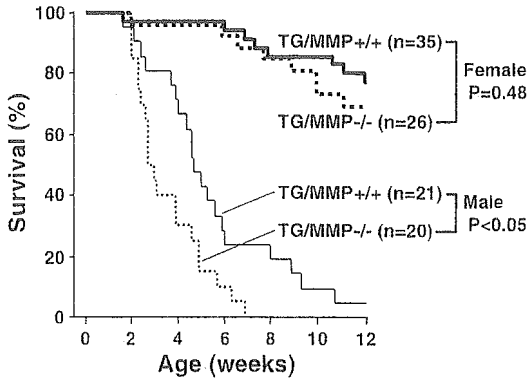


Fig. 3. Kaplan-Meier survival analysis of survival in male TG/MMP$^{+/+}$ ($n$ = 21) and TG/MMP$^{-/-}$ ($n$ = 20) and female TG/MMP$^{+/-}$ ($n$ = 35) and TG/MMP$^{-/-}$ ($n$ = 26) mice.

female mice are shown in Table 1. Presence or absence of the MMP-2 gene did not affect baseline echocardiographic parameters in WT mice. LV end-diastolic diameter was significantly greater, and fractional shortening was significantly less in TG/MMP$^{+/+}$ than in WT mice. TG/MMP$^{-/-}$ mice exerted more impaired LV contractile function than TG/MMP$^{+/+}$ mice.

There was no significant difference in heart rate or LV end-diastolic pressure (EDP) between WT/MMP$^{+/+}$ and WT/MMP$^{-/-}$ mice. LV EDP increased slightly, but significantly, in TG/MMP$^{+/+}$ mice and further increased in TG/MMP$^{-/-}$ mice. Consistent with LV EDP, pleural effusion was observed only in TG/MMP$^{-/-}$ mice. On the basis of these results, the exacerbation of heart failure might contribute to premature death in TG/MMP$^{-/-}$ mice.

*Histopathology.* We examined the histopathology of the heart from 12-wk-old female mice. LV weight was significantly increased in the TG groups compared with the WT groups (Table 1); however, LV weight did not differ between TG/MMP$^{+/+}$ and TG/MMP$^{-/-}$ mice. Furthermore, myocyte cross-sectional area and collagen volume fraction were increased in TNF-α TG groups (Fig. 4, *A* and *B*). However, the extent of these histopathological changes was comparable between TG/MMP$^{+/+}$ and TG/MMP$^{-/-}$ mice. Moreover, in picrosirius red-stained sections, the structure of the interstitial collagen fibers was similar between TG/MMP$^{+/+}$ and TG/MMP$^{-/-}$ mice (Fig. 4*C*), indicating that selective disruption of the MMP-2 gene did not alter collagen content or structure in this mouse model.

The number of infiltrating interstitial cells in the myocardium was greater in TNF-α TG than in WT mice (Fig. 5). The extent of infiltration was significantly greater in TG/MMP$^{-/-}$ than TG/MMP$^{+/+}$ mice. Macrophages infiltrated into the myocardium from TG mice, and, importantly, selective MMP-2 ablation further augmented their infiltration (Fig. 6).

*Cytokine gene expression.* TNF-α gene expression was significantly upregulated in the TNF-α TG myocardium (Fig. 7). In addition, overexpression of the TNF-α gene increased expression of other cytokines and chemokines, including RANTES, IL-6, IL-1β, and MCP-1, indicating that overexpression of TNF-α induced "downstream" cytokines and chemokines in this model. Importantly, upregulation of TNF-α was not altered by ablation of the MMP-2 gene. Similarly, MMP-2 gene ablation in TG mice had no significant effects on myo-

Table 1. *Characteristics of animal models*

| | WT/MMP$^{+/+}$ ($n$ = 15) | WT/MMP$^{-/-}$ ($n$ = 15) | TG/MMP$^{+/+}$ ($n$ = 15) | TG/MMP$^{-/-}$ ($n$ = 17) |
|---|---|---|---|---|
| Echocardiographic data | | | | |
| Heart rate, beats/min | 450±11 | 446±10 | 452±12 | 453±11 |
| LV EDD, mm | 3.4±0.1 | 3.3±0.1 | 4.3±0.1* | 4.5±0.2* |
| Fractional shortening, % | 37.4±0.8 | 36.8±0.7 | 26.7±0.9* | 22.9±1.3*† |
| Hemodynamic data | | | | |
| Heart rate, beats/min | 471±10 | 469±10 | 460±9 | 459±8 |
| LV EDP, mmHg | 0.5±0.7 | 0.2±0.3 | 1.5±0.7* | 7.2±2.5*† |
| Organ weight data | | | | |
| Body wt, g | 20.7±0.5 | 19.2±0.4 | 21.7±0.4 | 20.7±0.5 |
| LV wt/body wt, mg/g | 3.0±0.1 | 2.9±0.0 | 3.8±0.1* | 3.9±0.2* |
| Pleural effusion, % | | | 0 | 18 |

Values are means ± SE. WT/MMP$^{+/+}$, wild-type mice with matrix metalloproteinase-2 (MMP-2); WT/MMP$^{-/-}$, wild-type mice with MMP-2 knockout; TG/MMP$^{+/+}$, transgene (TG) mice with cardiac overexpression of TNF-α with MMP-2; TG/MMP$^{-/-}$, TG mice with cardiac overexpression of TNF-α with MMP-2 knockout; LV, left ventricular; EDD, end-diastolic diameter; EDP, end-diastolic pressure. *$P$ < 0.01 vs. WT/MMP$^{+/+}$. †$P$ < 0.05 vs. TG/MMP$^{+/+}$.

cardial mRNA levels of other cytokines/chemokines, indicating that the decline in survival and LV function in TG/MMP$^{-/-}$ mice was not due to enhancement of myocardial cytokine/chemokine expression by selective disruption of the MMP-2 gene.

*Plasma cytokine and MMP levels.* Plasma levels of TNF-α, as well as other cytokines, were below detection in the four groups of animals (Table 2), consistent with previous studies demonstrating that the TNF-α TG transcripts were limited to the heart (16). As expected, plasma levels of MMP-2 were very low in MMP-2 KO mice. Plasma MMP-2 was comparable between WT/MMP$^{+/+}$ and TG/MMP$^{+/+}$ mice.

## DISCUSSION

In the present study, we demonstrated that selective disruption of the MMP-2 gene exacerbated survival and LV function in TG mice with cardiac-specific overexpression of TNF-α. Disruption of the MMP-2 gene did not alter myocardial hypertrophy and interstitial fibrosis but exacerbated inflammatory cell infiltration. These results indicate that MMP-2 plays a protective role against myocardial inflammation and dysfunction in cytokine-induced cardiomyopathy.

Consistent with previous studies (17, 18), MMP-2 mRNA and activities were upregulated in myocardium from animals with TNF-α-induced cardiomyopathy (Figs. 1 and 2). Although the mechanisms responsible for this activation remain to be determined, cellular constituents of cardiac muscle, including fibroblasts, inflammatory cells, and myocytes, are known to be capable of expressing MMP-2 in response to specific stimuli (25). Activation of MMPs may be involved in the remodeling process of the failing heart by provoking alterations of the ECM (4, 8, 20, 23, 26, 27). Indeed, MMP-9 disruption reduced myocardial remodeling and improved LV function and survival rate after myocardial infarction (9). Similarly, MMP-2 ablation inhibited cardiac rupture and remodeling after myocardial infarction (8).

The present study investigated the long-term effects of selective MMP-2 gene disruption on development of TNF-α-induced cardiomyopathy. We employed KO mice, because selective MMP-2 inhibitors are not available and "selective" MMP-2 disruption is possible only with a KO mouse model. As expected, no MMP-2 expression was observed in myocardium from WT/MMP$^{-/-}$ and TG/MMP$^{-/-}$ mice (Figs. 1 and

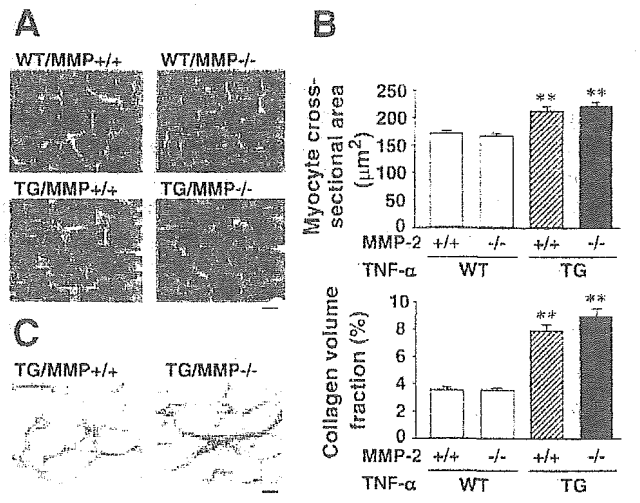


Fig. 4. *A*: representative high-power photomicrographs of Masson's trichrome-stained LV cross sections from WT/MMP$^{+/+}$, WT/MMP$^{-/-}$, TG/MMP$^{+/+}$, and TG/MMP$^{-/-}$ mice. Scale bar, 10 μm. *B*: summary data of myocyte cross-sectional area and collagen volume fraction by histopathological analysis of LV tissue sections ($n$ = 6/group). Values are means ± SE. **$P$ < 0.01 vs. WT/MMP$^{+/+}$. *C*: representative high-power photomicrographs of picrosirius red-stained LV cross sections from TG/MMP$^{+/+}$ and TG/MMP$^{-/-}$ mice. Scale bar, 10 μm.

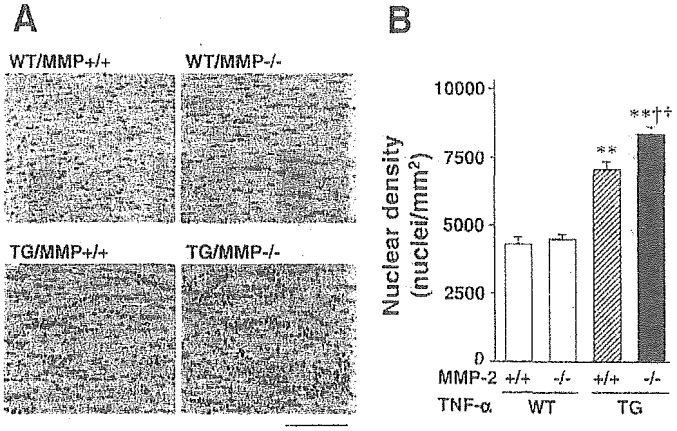


Fig. 5. *A*: representative photomicrographs of hematoxylin-and-eosin-stained LV sections from WT/MMP$^{+/+}$, WT/MMP$^{-/-}$, TG/MMP$^{+/+}$, and TG/MMP$^{-/-}$ mice. Scale bar, 100 μm. *B*: summary data for nuclear density of infiltrating cells ($n$ = 6/group). Values are means ± SE. **$P$ < 0.01 vs. WT/MMP$^{+/+}$. ††$P$ < 0.01 vs. TG/MMP$^{+/+}$.

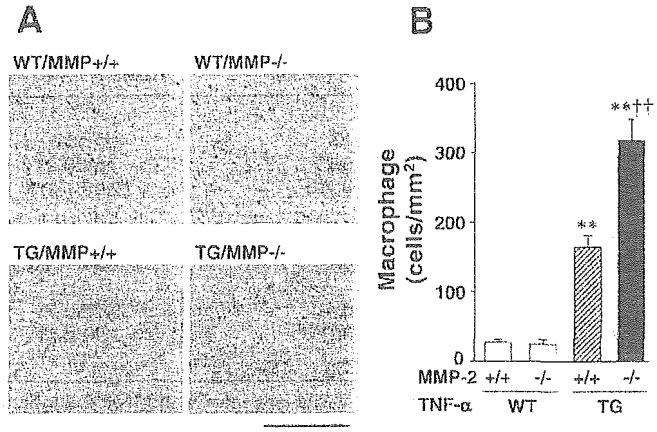


Fig. 6. *A*: representative photomicrographs of anti-Mac-3 antibody-stained LV sections from WT/MMP$^{+/+}$, WT/MMP$^{-/-}$, TG/MMP$^{+/+}$, and TG/MMP$^{-/-}$ mice. Scale bar, 100 μm. *B*: summary data for density of Mac-3-positive cells ($n$ = 5/group). Values are means ± SE. **$P < 0.01$ vs. WT/MMP$^{+/+}$. ††$P <$ 0.01 vs. TG/MMP$^{+/+}$.

2). We had expected that MMP-2 disruption could ameliorate cardiac ECM remodeling and dysfunction in TNF-α TG mice and prolong survival. On the contrary, selective blockade of the MMP-2 gene exacerbated LV contractile dysfunction and failure (Table 1) and even shortened survival (Fig. 3), suggesting that myocardial induction of MMP-2 may play a protective role against the development of cytokine-induced cardiomyopathy.

The most striking finding of the present study was an increase in inflammatory cell recruitment into the myocardium seen in MMP-2 KO mice due to overexpression of TNF-α in the heart (Figs. 5 and 6). Even though the pathophysiological significance of cellular infiltrates in myocardial remodeling and failure remains mostly speculative in this model, the observed increase in inflammation might exacerbate myocardial contractile and structural defects, which could lead to premature death

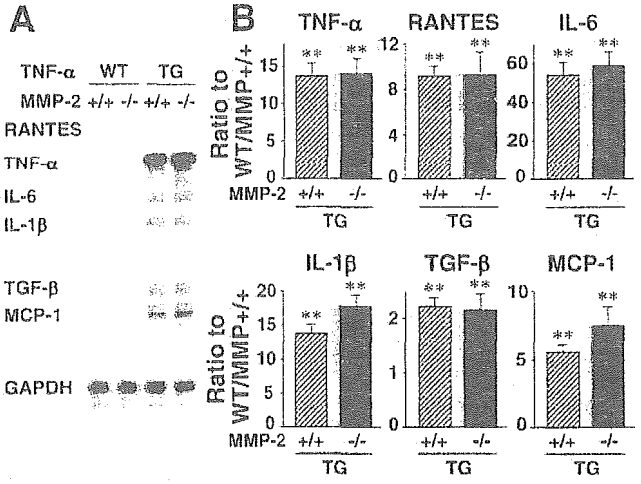


Fig. 7. *A*: myocardial gene expression of proinflammatory cytokines and chemokines from WT/MMP$^{+/+}$, WT/MMP$^{-/-}$, TG/MMP$^{+/+}$, and TG/MMP$^{-/-}$ mice. *B*: densitometric analysis of gene expression in myocardium from TG/MMP$^{+/+}$ ($n$ = 7) and TG/MMP$^{-/-}$ ($n$ = 6) mice. Each value was normalized to that of GAPDH in each template set as an internal control and expressed as ratio to WT/MMP$^{+/+}$ ($n$ = 6). MCP, monocyte chemoattractant protein; TGF, transforming growth factor; RANTES, regulated on activation, normal T cell expressed and secreted. Values are means ± SE. **$P < 0.01$ vs. WT/MMP$^{+/+}$.

Table 2. *Plasma levels of cytokines and MMPs*

| | WT/MMP$^{+/+}$ | WT/MMP$^{-/-}$ | TG/MMP$^{+/+}$ | TG/MMP$^{-/-}$ |
|---|---|---|---|---|
| Cytokines/chemokines | | | | |
| TNF-α, pg/ml | ND | ND | ND | ND |
| IL-6, pg/ml | 9.0±0.2 | 9.0±0.8 | 9.0±0.6 | 10.4±2.5 |
| IL-1β, pg/ml | ND | ND | ND | ND |
| MCP-1, pg/ml | 20.7±10.2 | 8.3±3.2 | 17.3±3.3 | 24.9±6.3 |
| MMP | | | | |
| MMP-2, ng/ml | 60.9±3.0 | 0.9±0.2* | 63.2±2.5 | 0.8±0.2* |

Values are means ± SE; $n$ = 5. ND, not detectable; MCP, monocyte chemoattractant protein. *$P < 0.01$ vs. WT/MMP$^{+/+}$.

in TG/MMP$^{-/-}$ mice. Several potential mechanisms of MMP-2 deletion are responsible for exacerbating cellular inflammation in TNF-α TG hearts. One possible mechanism is a further increase in expression of the TNF-α gene in TG/MMP$^{-/-}$ mice and the resultant enhancement of inflammation. However, this possibility is less likely, because the gene expression of cytokines, TNF-α and MCP-1, was not altered by selective disruption of the MMP-2 gene (Fig. 7), perhaps in part because expression of TNF-α in TG mice is driven by α-myosin heavy chain promoter, which is supposed to be MMP-2 independent. Another possibility is that MMP-2 might alter the milieu of the ECM, which could accelerate the infiltration of cells. In the present study, no significant changes were observed in collagen deposition between TG/MMP$^{+/+}$ and TG/MMP$^{-/-}$ mice (Fig. 4). Therefore, exacerbation of myocardial inflammation in TG/MMP$^{-/-}$ mice was not due to impairment of interstitial collagen formation and/or structure.

Theoretically, an increase in MMP activity would result in a decrease in the MMP substrate, collagen, whereas inhibition of MMP-2 would result in an increase in collagen. However, in agreement with previous studies (18), the present study demonstrated that an increase in MMP-2 activity was accompanied by an increase in fibrosis in TNF-α TG mice (Fig. 4). Moreover, selective disruption of the MMP-2 gene did not alter these changes in interstitial fibrosis. The present study could not provide a definite explanation for these paradoxical findings, perhaps because total ECM collagen content is a complex function of synthesis and degradation.

Although the functional role of MMP-2 in this aspect and its significance in myocardial inflammation remain unknown, on the basis of a previous study by Heymans et al. (9), we could not exclude the possibility that deletion of the MMP-2 gene might alter ECM components other than collagens, disrupt the alignment of myocytes with the ECM or degrade the ECM surrounding the myocytes, and promote the further progression of inflammatory cell migration into the interstitial space. MMPs have been shown to facilitate inflammatory cell recruitment (7). However, the present study does not provide a direct proof for the cause-and-effect relation between the increase in cellular infiltration and the exacerbation of heart failure, and further investigation is clearly needed.

The results of the present study are consistent with those of previous studies of MMP-2 gene ablation in other models of tissue inflammation (3, 13). Disruption of the MMP-2 gene exacerbated allergic lung inflammation and increased lethal susceptibility to asphyxiation in a mouse model of asthma (3). Furthermore, Itoh et al. (13) demonstrated an increase in severity of arthritis in association with tissue inflammation in